Spatially heterogeneous diapycnal mixing in the abyssal ocean: A comparison of two parameterizations to observations

Thomas Decloedt[1] and Douglas S. Luther[1]

Received 21 June 2012; revised 1 October 2012; accepted 2 October 2012; published 28 November 2012.

[1] The spatial distributions of the diapycnal diffusivity predicted by two abyssal mixing schemes are compared to each other and to observational estimates based on microstructure surveys and large-scale hydrographic inversions. The parameterizations considered are the tidal mixing scheme by Jayne, St. Laurent and co-authors (JSL01) and the Roughness Diffusivity Model (RDM) by Decloedt and Luther. Comparison to microstructure surveys shows that both parameterizations are conservative in estimating the vertical extent to which bottom-intensified mixing penetrates into the stratified water column. In particular, the JSL01 exponential vertical structure function with fixed scale height decays to background values much nearer topography than observed. JSL01 and RDM yield dramatically different horizontal spatial distributions of diapycnal diffusivity, which would lead to quite different circulations in OGCMs, yet they produce similar basin-averaged diffusivity profiles. Both parameterizations are shown to yield smaller basin-mean diffusivity profiles than hydrographic inverse estimates for the major ocean basins, by factors ranging from 3 up to over an order of magnitude. The canonical 10^{-4} m^2 s^{-1} abyssal diffusivity is reached by the parameterizations only at depths below 3 km. Power consumption by diapycnal mixing below 1 km of depth, between roughly 32°S and 48°N, for the RDM and JSL01 parameterizations is 0.40 TW & 0.28 TW, respectively. The results presented here suggest that present-day mixing parameterizations significantly underestimate abyssal mixing. In conjunction with other recently published studies, a plausible interpretation is that parameterizing the dissipation of bottom-generated internal waves is not sufficient to approximate the global spatial distribution of diapycnal mixing in the abyssal ocean.

Citation: Decloedt, T., and D. S. Luther (2012), Spatially heterogeneous diapycnal mixing in the abyssal ocean: A comparison of two parameterizations to observations, *J. Geophys. Res.*, *117*, C11025, doi:10.1029/2012JC008304.

1. Introduction and Motivation

[2] The spatial distribution of turbulent diapycal mixing in the deep ocean is strongly influenced by seafloor topography. Rough topography can act as a site of internal wave generation, scattering and reflection, thereby energizing the internal wavefield in its vicinity [e.g., *Wunsch and Webb*, 1979]. An energized internal wavefield, especially if energized at small scales, is more prone to shear instability, the latter generally being assumed to be the dominant source of turbulence leading to diapycnal mixing in the abyssal ocean [e.g., *Toole*, 1998; *Polzin*, 2004]. Significant mixing is also associated with deep flow through bathymetric constrictions such as canyons and fracture zones [e.g., *Polzin et al.*, 1996; *Thurnherr et al.*, 2005]. Flows through gaps containing sills may accelerate due to gravity, develop shear instability, generate internal lee waves and/or be subjected to hydraulic jumps leading to intense mixing [*Toole*, 1998].

[3] Estimates of diapycnal mixing based on tracer-release experiments, microstructure measurements and a variety of fine-scale techniques consistently infer background values of the diapycnal diffusivity, $K_\rho \sim O(10^{-5}$ m^2 s$^{-1})$, in the deep ocean interior away from rough topography and away from strongly sheared flow such as the Equatorial Undercurrent System [e.g., *Gregg*, 1987; *Ledwell et al.*, 1993; *Kunze and Sanford*, 1996; *Ledwell et al.*, 2011]. Bottom-intensified diffusivities several orders of magnitude greater than background values are commonly inferred over regions of rough topography such as seamounts [*Lueck and Mudge*, 1997; *Toole et al.*, 1997; *Carter et al.*, 2006], ridges [*Polzin et al.*, 1997; *Althaus et al.*, 2003; *Aucan et al.*, 2006; *Klymak et al.*, 2008], canyons and fracture zones [*Ferron et al.*, 1998; *Carter and Gregg*, 2002; *Thurnherr et al.*, 2005; *MacKinnon et al.*, 2008]. The spatial distribution of diapycnal mixing is thus heterogeneous: patchy in the horizontal and a function of height above bottom in the vertical.

[4] In contrast, Ocean General Circulation Models (OGCMs) traditionally use a variant of the *Bryan and Lewis* [1979] parameterization which is uniform in the horizontal

[1]SOEST, University of Hawai'i at Mānoa, Honolulu, Hawai'i, USA.

Corresponding author: T. Decloedt, SOEST, University of Hawai'i at Mānoa, Marine Sciences Building, 1000 Pope Rd., Honolulu, HI 96822, USA. (decloedt@hawaii.edu)

0148-0227/12/2012JC008304

and depth-dependent (e.g., the Community Climate Simulation Model (CCSM) [see *Jayne*, 2009] and LOVECLIM [*Goosse et al.*, 2010]). More sophisticated parameterizations exist, mostly gradient Richardson number dependent (e.g., the interior part of KPP by *Large et al.* [1994] and *Jackson et al.* [2008]). Short of running at unrealistically high resolutions supporting the internal wavefield, these parameterizations effectively result in laterally homogeneous mixing in the deep ocean.

[5] In recent decades, the interest in observations of spatially heterogeneous mixing due to rough topography stemmed in large part from a desire to reconcile the order of magnitude difference between the weak, observed values of mixing in the ocean interior with the canonical 10^{-4} m^2 s^{-1} required in the seminal *Munk* [1966], and later *Munk and Wunsch* [1998], "Abyssal Recipes" papers. *Robinson and Stommel* [1959] and *Wyrtki* [1961] also arrived at a value of 10^{-4} m^2 s^{-1} in their work on the thermohaline and abyssal circulation. Note that the "Abyssal recipes" papers were focused on the "bathyal" zone between 1 km and 4 km depth, not the "abyssal" zone between 4 km and 6 km; however, the term "abyssal" commonly now refers to all ocean depths below the thermocline, and will be used as such throughout this paper. Based on the concept of a vertical balance between advection and diffusion, these papers argued that a diffusivity of that magnitude is required to maintain the abyssal density stratification against the continual influx of bottom waters formed at high latitudes. A compelling link was made between the power available for diapycnal mixing in the abyssal ocean and the strength of the Meridional Overturning Circulation (MOC), its associated heat transport and thus climate state. Indeed, combining the assumption of a 1-D advective-diffusive balance with the continuity and thermal wind equations, the meridional mass transport can be shown to be proportional to $K_\rho^{1/3}$ [e.g., *Bryan*, 1987; *Marotzke*, 1997]. One could thus argue that the $\sim$2 petawatts poleward heat flux associated with the MOC cannot exist without the relatively minute power sources (a few terawatts from winds and tides) providing the mechanical energy for continuous turbulent mixing of the abyssal ocean.

[6] The concept of a simple link between climate state, the MOC and diapycnal mixing in the abyssal ocean is now slowly being abandoned. This shift is in large part thanks to the use of OGCMs as a tool to test the sensitivity of the large-scale circulation to the spatial heterogeneity of small-scale turbulent mixing. *Saenko* [2006] and *Jayne* [2009] show that simple scaling relations connecting the strength of the MOC to diapycnal mixing break down in the case of spatially heterogeneous mixing. Likewise, low-resolution sensitivity experiments by *Jayne* [2009] and *Ferrari and Ferreira* [2011] indicate only a weak connection between poleward oceanic heat transport (OHT) and abyssal mixing while exhibiting a stronger relation between OHT and diapycnal mixing at thermocline depths.

[7] Numerical sensitivity studies show a large variety of ocean characteristics other than the OHT to be sensitive to the heterogeneity of K_ρ in the abyssal ocean however, for instance the deep overturning cell and abyssal circulation [*Huang and Jin*, 2002; *Saenko and Merryfield*, 2005; *Katsman*, 2006] the large-scale potential vorticity distribution [*Saenko and Merryfield*, 2005], water mass properties [*Koch-Larrouy et al.*, 2007; *Harrison and Hallberg*, 2008] and the depth and intensity of the Antarctic Circumpolar Current (ACC) [*Saenko*, 2006; *Jayne*, 2009; *Friedrich et al.*, 2011]. In addition, abyssal heterogeneous mixing has a significant effect on marine biogeochemistry, in particular Primary Productivity and the extent of Oxygen Minimum Zones [*Duteil and Oschlies*, 2011; *Friedrich et al.*, 2011]. In coupled air-sea models, heterogeneous mixing alters the sea surface temperatures and therefore the atmospheric circulation [*Richards and Xie*, 2009; *Müller et al.*, 2010; *Friedrich et al.*, 2011]. Importantly, these properties are not only influenced by the different horizontally averaged mixing rates but depend on details of the horizontal distribution [e.g., *Simmons et al.*, 2004; *Friedrich et al.*, 2011] and the vertical structure [e.g., *Saenko et al.*, 2012].

[8] Given the large number of ocean characteristics depending on both the vertical and horizontal distributions of K_ρ, parameterizations that capture the spatial (and ultimately temporal) variation of diapycnal mixing without the explicit need to resolve the internal wavefield are crucial if we are to have confidence in OGCM simulations. While this has long been recognized [e.g., *Wunsch and Ferrari*, 2004], present-day heterogeneous mixing parameterizations remain preliminary and have been subjected to little validation. In an effort to gauge the realism and identify shortcomings of these preliminary heterogeneous mixing parameterizations, we here compare and contrast two such schemes against each other and against observations.

[9] The parameterizations considered here are the tidal mixing parameterization [*Jayne and St. Laurent*, 2001; *St. Laurent et al.*, 2002, hereinafter referred to as JSL01], used in the vast majority of the sensitivity studies mentioned earlier, and the Roughness Diffusivity Model [*Decloedt and Luther*, 2010, hereinafter referred to as RDM]. These represent idealized extremes for the volume of the abyssal ocean influenced by the breaking of bottom-generated internal waves; the JSL01 being a minimum, prescribing enhanced mixing only in regions of combined rough topography and tidal forcing, and the RDM a maximum, prescribing enhanced mixing over all rough topography.

[10] The JSL01 and RDM are compared against (i) diffusivities estimated from inversions of hydrography for the major ocean basins, and (ii) microstructure-based estimates for the Hawaiian Ridge and Brazil Basin areas. Diffusivity estimates based on fine-scale parameterizations such as the Gregg-Henyey scaling [*Gregg et al.*, 2003] are not included in the comparison because of serious concerns regarding the robustness of the method, particularly in weakly stratified waters such as the abyssal ocean considered here [*Kunze et al.*, 2006; *Waterman et al.*, 2012] For example, *Kunze et al.* [2006] found shear variance to be dominated by instrument noise for buoyancy frequencies $N < 5 \times 10^{-4}$ rad s^{-1}, corresponding to depths roughly greater than 1000 m at midlatitudes and argues that this led *Garabato et al.* [2003] to overestimate mixing by an order of magnitude in the deep Scotia Sea. Recent microstructure measurements in the Southern Ocean were found to be much more modest than expectations based on fine-scale parameterizations, typically by factors of 4–5 [*Waterman et al.*, 2012]. Up to an order of magnitude difference between dissipation rate estimates by *Huussen et al.* [2012] and *Kunze et al.* [2006] have been noted, in spite of both studies

nominally using the same data and technique (K. Polzin, personal communication, 2012).

[11] This paper is organized as follows. In section 2, the JSL01 and RDM parameterizations are described in more detail. In section 3, their spatial distributions are contrasted against each other and shown to be dramatically different which would lead to quite different circulations in OGCMs, yet they yield similar basin-averaged diffusivities. In section 4, the parameterizations are shown to be biased low compared to basin-scale hydrographic inverse estimates of diffusivity. Comparison to microstructure surveys in section 5 shows that both parameterizations are also conservative in estimating the extent to which bottom-intensified mixing penetrates into the stratified water column, with the RDM being more agreeable. In section 6, the power consumed by the parameterized diffusivity distributions as well as the power consumption implied by the inverse estimates are computed. Finally, these results are summarized and discussed in section 7.

2. The JSL01 and RDM Parameterizations

2.1. JSL01 Tidally Forced Diapycnal Mixing

[12] The JSL01 parameterization [*Jayne and St. Laurent*, 2001; *St. Laurent et al.*, 2002] provides an estimate for the diapycnal diffusivity resulting from the breaking of locally generated high mode internal tides. The key term of the JSL01 parameterization is the geographical distribution of the rate of energy conversion $E(x, y)$ from the barotropic to baroclinic tides. This is the source term of energy available for turbulent dissipation and is computed as $E(x, y) \cong 1/2\rho N_b \kappa h^2 \langle u_{bt}^2 \rangle$ based on the work by *Bell* [1975] where ρ is a reference density, N_b the buoyancy frequency at the seafloor, κ and h are the wave number and amplitude scales for topographic roughness, and $\langle u_{bt}^2 \rangle$ the temporal mean square barotropic tidal velocity. The scaling for $E(x, y)$ was developed in *Jayne and St. Laurent* [2001] to represent tidal drag in hydrodynamical models of the barotropic tide. When implemented as an internal wave drag term, the energy flux scaling improved the fidelity of forward tide models with respect to estimates of tidal dissipation and root-mean square sea surface elevation inferred from satellite altimetry. The scaling applies to sub-critical topography but the modeling work of *Zilberman et al.* [2009] suggests the accuracy of the scaling could be well within a factor of 2 for critical and supercritical topography. The 2-D conversion term was then used as the starting point to estimate the 3-D distribution of the turbulent kinetic energy dissipation rate ε as

$$\varepsilon(x,y,z) = \frac{qE(x,y)F(z)}{\rho} \tag{1}$$

where $q = 0.3$ is the fraction of the energy flux assumed to dissipate locally and $F(z)$ is a vertical structure function for the TKE dissipation rate. The vertical structure function $F(z) = [e^{-(H+z)/\zeta}]/[\zeta(1 - e^{-H/\zeta})]$ satisfies $\int_{-H}^{0} F(z)dz = 1$ to ensure that a fraction q of the available energy flux is dissipated within the vertically integrated water column of depth $z = -H$. The vertical decay scale $\zeta = 500$ m is roughly based on fitting an exponential profile to the Brazil Basin microstructure survey. The JSL01 spatial distribution of the diapycnal diffusivity then follows from the *Osborn* [1980] relation, $K_\rho = \Gamma\varepsilon/N^2$, as

$$K_\rho(x,y,z) = \frac{q\Gamma E(x,y)F(z)}{\rho N^2} + K_0 \tag{2}$$

where $K_0 = 10^{-5}$ m^2 s^{-1} is an assumed background diffusivity and $\Gamma = 0.2$ is the mixing efficiency.

[13] An acknowledged concern with the JSL01 parameterization as it stands is its dependence on arbitrary constants. The parameters q and ζ are uncertain and likely functions of both space and time [*St. Laurent and Nash*, 2003; *Jayne*, 2009]. *Althaus et al.* [2003] estimated $q \sim 0.01$ along the ridge crest of the Mendocino Escarpment, indicating that q may have an order-of-magnitude spatial variability. Likewise, estimates of the vertical scale height ζ range from 150 m [*Polzin*, 2004] to 5000 m [*Kunze et al.*, 2006]. Horizontal circulation is influenced by vertical gradients of the diapycnal diffusivity and thus one can expect simulations to be sensitive to the choice of scale height, as was recently demonstrated by *Saenko et al.* [2012] and discussed in further detail later in section 5 of this paper.

[14] In terms of parameterizing diapycnal mixing in the abyssal ocean, the major weakness of JSL01 is that only a fraction of the internal wave energy available for mixing is represented. *St. Laurent et al.* [2002] clearly acknowledge this fact yet, in practice, JSL01 is often de facto implemented as a parameterization of total diapycnal mixing in the abyssal ocean. JSL01 has been implemented in various OGCMs such as the NCAR Community Climate System Model (CCSM) [*Saenko and Merryfield*, 2005; *Jayne*, 2009] and the GFDL Modular Ocean Model [*Simmons et al.*, 2004].

[15] Of the approximately 1 TW converted into baroclinic tides in the abyssal ocean, an estimated 0.3 TW [*St. Laurent et al.*, 2002] is dissipated locally. The remaining 0.7 TW of baroclinic tidal energy radiates away from internal tide generation sites as low modes [*Egbert and Ray*, 2000]. Some of this low mode energy is dissipated on distant continental slopes [*Nash et al.*, 2004], some bleeds into the ambient internal wavefield through wave-wave interactions [*Hibiya et al.*, 2002], some may scatter off deep ocean topography [e.g., *Johnston and Merrifield*, 2003], and a sizable fraction may dissipate in the upper ocean as it encounters stronger stratification and reflects off the surface [e.g., *Althaus et al.*, 2003]. The exact partition and fate of the low modes remains unknown. Suffice it to say that it is probable that substantially less than 1 TW is available from the tides for mixing the abyssal ocean.

[16] Other obvious, potentially important, non-tidal sources of mechanical energy are near-inertial internal waves and mesoscale eddies. *Alford* [2003] estimates that 0.5 TW of surface-generated near-inertial internal wave energy radiates into the deep ocean based on a slab model. How much of the near-inertial wave energy reaches the abyssal ocean remains uncertain. Numerical studies suggest that most of the near-inertial energy is dissipated in the upper few hundred meters [*von Storch et al.*, 2007; *Furuichi et al.*, 2008; *Hughes and Wilson*, 2008]. Interaction of near-inertial waves with internal tides may also remove a significant fraction of the near-inertial energy from the internal wave band before it

penetrates into the deep ocean [*Guiles*, 2009]. In contrast, anticyclonic eddies may act as conduits of near-inertial energy into the deep ocean as suggested by *Kunze* [1985]. *Jing et al.* [2011] present observational evidence for this effect and high-resolution, numerical studies now explore the role of eddies in transferring near-inertial energy to the deep ocean [e.g., *Zhai et al.*, 2005; *Danioux et al.*, 2008].

[17] Mesoscale eddies also likely play a more direct role in deep ocean mixing as suggested by the analysis of *Fu et al.* [1982] and *Gille et al.* [2000]. *Zhai et al.* [2010] estimate 0.1–0.3 TW is available for deep ocean mixing due to dissipation of eddies at western boundaries. *Nikurashin and Ferrari* [2011] investigate the dissipation of internal lee waves resulting from geostrophic eddies flowing over small-scale topography. They estimate a global energy conversion from geostrophic flow into internal waves of 0.2 TW, half of which occurs in the Southern Ocean.

[18] In addition, it is likely there exist a number of processes pumping mechanical energy into the abyssal ocean that are much less obvious and not yet quantified. For instance, in the western-central equatorial Atlantic and the central-eastern equatorial Pacific Ocean, there is good evidence for downward-propagating beams of monthly periodic Yanai (Rossby gravity) waves [*Weisberg et al.*, 1979; *Ascani et al.*, 2010]. As these beams propagate into the abyssal ocean, a fraction of their energy is converted into internal waves and may lead to diapycnal mixing in an area where internal-wave induced mixing is generally considered to be at a minimum [*Gregg et al.*, 2003]. In short, the mechanical energy available for diapycnal mixing is ill-constrained and it is conceivable that the diapycnal mixing parameterized by JSL01 represents less than half of the total mixing occurring in the abyssal ocean.

2.2. RDM (Roughness Diffusivity Model)

[19] The premise of the RDM [*Decloedt and Luther*, 2010] is that total topography-catalyzed internal wave driven mixing can be approximated as depending mainly on topographic roughness. This is rooted in an observed (albeit approximate) relation between ε and a simple roughness metric. The implicit, and as of yet unconfirmed, assumption is that the sum total of all energy sources and energy conversion processes contributing to topography-catalyzed mixing may have a more uniform horizontal dependence than any of the individual contributors. Examination of $\sim$300 microstructure-based diffusivity profiles from various geographical locations revealed that boundary diffusivities stratify according to a simple metric of topographic roughness [see *Decloedt and Luther*, 2010, Figure 5]. A correlation between diapycnal mixing and topographic roughness is also noted in for example *Kunze et al.* [2006], *Lozovatsky et al.* [2008], *Nikurashin and Ferrari* [2011], *Wu et al.* [2011], *Huussen et al.* [2012] and *Jing et al.* [2011]. The key term in the RDM is the geographical distribution of the maximum boundary diffusivities $K_b(r(x, y))$, assumed to be a function only of topographic roughness $r(x, y)$. The RDM is available online (http://www2.hawaii.edu/$\sim$decloedt/).

[20] Topographic roughness for the RDM is computed as the weighted RMS height of the *Smith and Sandwell* [1997] bathymetry. Note that different roughness metrics are used in the above cited studies, ranging from the topographic variance [e.g., *Kunze et al.*, 2006; *Wu et al.*, 2011] to mean square differences between 2-D polynomial fits and the bathymetry used. Most of the studies cited above use the *Smith and Sandwell* [1997] satellite altimetry based topography. A different roughness metric would yield different functional forms for both the boundary diffusivity K_b and the scale height, h_0, employed in the RDM. A higher resolution bathymetry would likely improve the relation between dissipation and roughness. *Polzin* [2004] and *Nikurashin and Ferrari* [2011] estimate topographic features with horizontal wavelengths of O(0.1–10 km) to be key in the generation of internal waves leading to dissipation over rough topography. These scales are well below the typical 10–20 km resolution of satellite altimetry. In an effort to resolve smaller roughness scales, *Nikurashin and Ferrari* [2011] propose a metric based on a combination of single beam ship soundings and the theoretical spectrum by *Goff and Jordan* [1988]. This approach potentially resolves scales of O(1 km) but suffers from unevenly distributed ship tracks and the issue that the *Goff and Jordan* [1988] spectrum targets abyssal hills formed by ridge-crest processes and may therefore not be representative of other topographic features such as seamounts and fracture zones. Along a similar vein, *Goff and Arbic* [2010] propose a statistical method to predict unresolved topographic roughness associated with abyssal hills. The utility of any given roughness metric will depend on its appropriateness for capturing the impact of topography on a particular topography-dependent process that contributes to mixing and/or on its success in predicting observed ε or K_ρ.

[21] Examination of the microstructure-based diffusivity profiles revealed a common vertical decay structure despite the variety of geographical locations [*Decloedt and Luther*, 2010]. The RDM vertical decay structure is a power law, providing a better fit to the observed diffusivity profile structures than exponential profiles and in line with the work by K. Polzin. *Polzin* [1999, 2004, 2009] developed a heuristic recipe for the TKE dissipation rate profile as a function of height above bottom assuming the TKE dissipation rate to be set by the interplay of upward-propagating, bottom-generated internal waves and the transport of energy down to dissipation scales via nonlinear wave-wave interactions. This type of vertical structure for the TKE dissipation rate may thus be expected to apply quite generally over topography, regardless of the specifics of the internal wave generation mechanism at hand. *Polzin* [2009] provides a recipe to implement his parameterization, albeit considering only tide-topography interaction. The *Polzin* [2009] parameterization has recently been implemented into an OGCM for the first time (A. Melet et al., Sensitivity of the ocean state to the vertical distribution of internal-tide driven mixing, submitted to *Journal of Physical Oceanography*, 2012).

[22] The 3-D RDM spatial distribution for the diapycnal diffusivity is

$$K_\rho(h, r(x,y)) = K_b(r)(1 + h/h_0(r))^{-2} + K_0, \qquad (3)$$

where h is height above bottom. The boundary diffusivity $K_b(r)$ and decay scale $h_0(r)$ are simple polynomial functions of topographic roughness $r(x, y)$ whose coefficients were determined empirically via nonlinear regressions of (3) on the microstructure-derived diffusivities. As in the numerical work by *Iwamae et al.* [2012], a trade-off relationship was

found between the near-boundary mixing intensity and the vertical decay scale, with large boundary mixing corresponding to decay scales of $O(100$ m) and weak boundary mixing with decay scales of $O(1000$ m). The dependence of the decay scale on topographic roughness differs from the JSL01 scheme in which the vertical decay scale is simply a constant. The background diffusivity $K_0 = 5.6 \times 10^{-6}$ m^2 s^{-1} also differs from JSL01, being the diffusivity that can be sustained by the Garret-Munk internal wavefield [*Polzin et al.*, 1995]. This choice of background diffusivity allows the modeled diffusivity to be less than 10^{-5} m^2 s^{-1}, often considered to be a reasonable background value in the open ocean [e.g., *Munk and Wunsch*, 1998]. In fact, diffusivities estimated from microstructure data [e.g., *Ledwell et al.*, 2011] and the many diffusivities estimated by *Kunze et al.* [2006] are frequently smaller than 10^{-5} m^2 s^{-1} away from rough topography. *Jayne* [2009] adds that background mixing may need to be made a function of space to account for processes that effect energy transfers to small scales independent of topography, such as parametric subharmonic instability (PSI) at critical latitudes [*MacKinnon and Winters*, 2005; *Alford et al.*, 2007] and other latitudinal changes in the distribution of internal wave energy dissipation [*Gregg et al.*, 2003; *Hibiya et al.*, 2006; *Jochum*, 2009]. *Duteil and Oschlies* [2011], using the JSL01 parameterization, recently demonstrated the sensitivity of OGCM solutions to the value of background mixing.

[23] The RDM has been implemented in LOVECLIM, an Earth System Model of Intermediate Complexity. *Friedrich et al.* [2011] investigated the effect of heterogeneous diapycnal mixing on ocean and atmosphere circulation as well as marine biogeochemistry and concluded that topography-enhanced mixing has a noticeable and global impact.

[24] A physically unsatisfying aspect of the implementation of the RDM in OGCMs is that the diapycnal diffusivity is parameterized directly rather than the more physical approach of parameterizing first the TKE dissipation rate and then computing the resulting turbulent diffusivity using the *Osborn* [1980] relation with the model-generated stratification. A dependence on model-generated stratification would allow for the diffusivity field to evolve with changing conditions, a desirable feature particularly for paleoclimate studies where both the source of energy available for mixing and the global stratification may have been considerably different from present-day conditions [e.g., *Green et al.*, 2009]. The choice to cast the RDM in terms of diffusivity was motivated by the *Henyey et al.* [1986] wave-wave interaction model. *Polzin et al.* [1995] examined several such models against micro- and fine structure data and found the most support for the *Henyey et al.* [1986] model, implying that $\varepsilon \propto N^2$. Direct numerical simulation of internal wave energy transfer in the midlatitude thermocline also provides support for the $\varepsilon \propto N^2$ scaling [e.g., *Winters and D'Asaro*, 1997]. Given the Osborn relation, $K_\rho = \Gamma\varepsilon/N^2$, the diapycnal diffusivity is then in theory independent of the stratification [*Toole*, 1998]. The Henyey model applies to the energy flux through the Garret-Munk (GM) internal wavefield [*Garrett and Munk*, 1972] and should yield a reasonable estimate for the background internal wavefield. Near topography, however, the internal wavefield can deviate considerably from the GM description [e.g., *Wunsch and Webb*, 1979; *Kunze et al.*, 2006; *Klymak et al.*, 2008], and it is unclear how applicable the Henyey model is in this situation.

3. Comparison of JSL01 and RDM Diffusivity Distributions

[25] Figures 1, 2, and 3 show the global distributions of the JSL01 and RDM diapycnal diffusivities at the bottom boundary, 3000 m and 1000 m of depth respectively. The 3-D distributions were computed at the $0.5^\circ \times 0.5^\circ$ degree, 45 depth levels grid spacing used for the World Ocean Circulation Experiment (WOCE) climatology [*Gouretski and Koltermann*, 2004]. The internal tide energy flux $E(x, y)$ was obtained courtesy of S. Jayne and is the one used in the CCSM3 experiments in *Jayne* [2009]. The N^2 distribution was computed from the *Gouretski and Koltermann* [2004] climatology temperature and salinities. *Simmons et al.* [2004] constrain JSL01 diffusivities in the limit of $N \rightarrow 0$ by setting N^2 to be larger than 10^{-8} s^{-2} whereas *Jayne* [2009] and *Saenko and Merryfield* [2005] cap the diffusivities at 10^{-1} m^2 s^{-1} and 2×10^{-3} m^2 s^{-1} respectively. In the following, the minimum N^2 is simply constrained to be greater than f^2 since f^2 is nominally the minimum frequency for freely propagating internal gravity waves [*LeBlond and Mysak*, 1978]. This cutoff only needed to be applied at a few points, mostly in the deep North Pacific. Where this was the case, JSL01 diffusivities were set to background values.

[26] The bottom panels of Figures 1–3 show the ratios of the RDM to the JSL01 diffusivities. It is clear that the difference between the two parameterizations is most pronounced in the Southern Hemisphere. In particular, diffusivities differ by up to 2–3 orders of magnitude over the Southeast Indian Ridge south of Australia and the Pacific-Antarctic Ridge. Both these areas have rough topography but weak tidal forcing. Few measurements exist in these areas for validation purposes. The work by *Polzin and Firing* [1997] along WOCE section I8S (Broken Plateau down to Kerguelen Plateau) is an area where the RDM and JSL01 differ significantly. *Polzin and Firing* [1997] infer diffusivities reaching 10^{-4} m^2 s^{-1} near the bottom at 35°S. This is consistent with the RDM but JSL01 diffusivities are near background levels at that location. Further south near the Kerguelen Plateau, *Polzin and Firing* [1997] infer near-bottom diffusivities of $O(10^{-3}$ m^2 s$^{-1})$, remaining well above 10^{-4} m^2 s^{-1} below a 1000 m of depth which they attribute to enhanced internal wave shear resulting from eddy currents, not tides. Both parameterizations predict strong bottom-diffusivities but neither predicts enhanced diffusivities to be sustained that far from the bottom.

[27] At 3000 m and 1000 m of depth (Figures 2 and 3), the effect of the different vertical structure functions used in the JSL01 and RDM parameterizations becomes apparent. The exponential decay with fixed scale height of 500 m used in JSL01 calls for a much faster decay of bottom-intensified mixing to background values than is the case for the RDM. The scale height used in the RDM is location dependent, ranging from ~650 m (slow) to ~150 m (fast) over smooth and rough topography respectively. As in *Polzin* [2004], the decay goes as an inverse square law with height above bottom. At 3000 m of depth, the JSL01 predicts ~60% of the ocean area to have diffusivities at the background value compared to only 17% for the RDM. At 1000 m of depth,

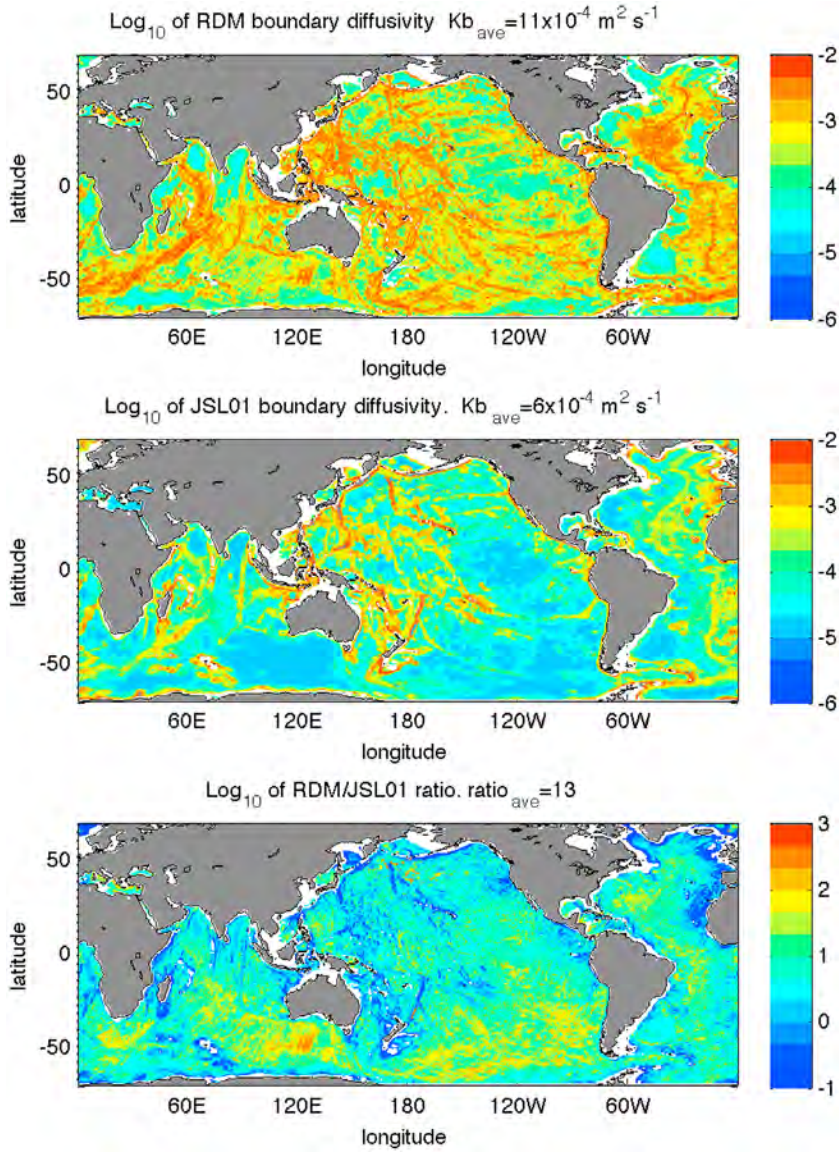

Figure 1. RDM and JSL01 diffusivities at the bottom boundary. At the top of each frame is the averaged diffusivity at the bottom for the entire domain (70°N-70°).

~90% of the JSL01 diffusivities are at the background level compared to ~50% for the RDM (see Tables 1a and 1b, top of second columns). The JSL01 diffusivities at 1000 m depth have become quasi-homogeneous in the horizontal whereas the RDM predictions remain patchy. In other words, the RDM predicts the influence of topography-catalyzed mixing in the abyssal ocean to extend much higher into the water column, even into the thermocline, than does the JSL01. *Jayne* [2009] and *Ferrari and Ferreira* [2011] show that the oceanic heat transport in OGCMs is very sensitive to mixing values at thermocline depths, the latter clearly a function of scale height, or how fast bottom-intensified mixing decays with height above bottom.

[28] In spite of the different distributions of diffusivities predicted by the RDM and JSL01, mean diffusivity magnitudes at a given depth level are surprisingly close, generally within a factor of two. Mean values are shown above each panel of Figures 1–3. Due to the quasi-lognormal distribution of diapycnal diffusivity, arithmetic mean values are very sensitive to the highest diffusivity values. This is particularly clear at the 1000 m depth level where the mean JSL01 diffusivity is in fact slightly higher than the mean RDM diffusivity (4×10^{-5} m^2 s^{-1} compared to 3×10^{-5} m^2 s^{-1} for the RDM), in spite of ~90% of the JSL01 diffusivities being at background levels compared to only ~50% for the RDM. The RDM maximum diffusivity value is set by the empirical function relating boundary diffusivity to topographic roughness and is 5.3×10^{-3} m^2 s^{-1}. Many measurements are much greater than this value of course, but the RDM seeks to describe the time-mean diffusivity at a given location. In the case of JSL01, the maximum diffusivity is very much a function of what criteria are used to constrain the minimum buoyancy frequency. For the criteria used here (see opening paragraph of this section), the maximum JSL01 boundary diffusivity is 2.5×10^{-1} m^2 s^{-1}. Mean diffusivity values therefore provide little information as to

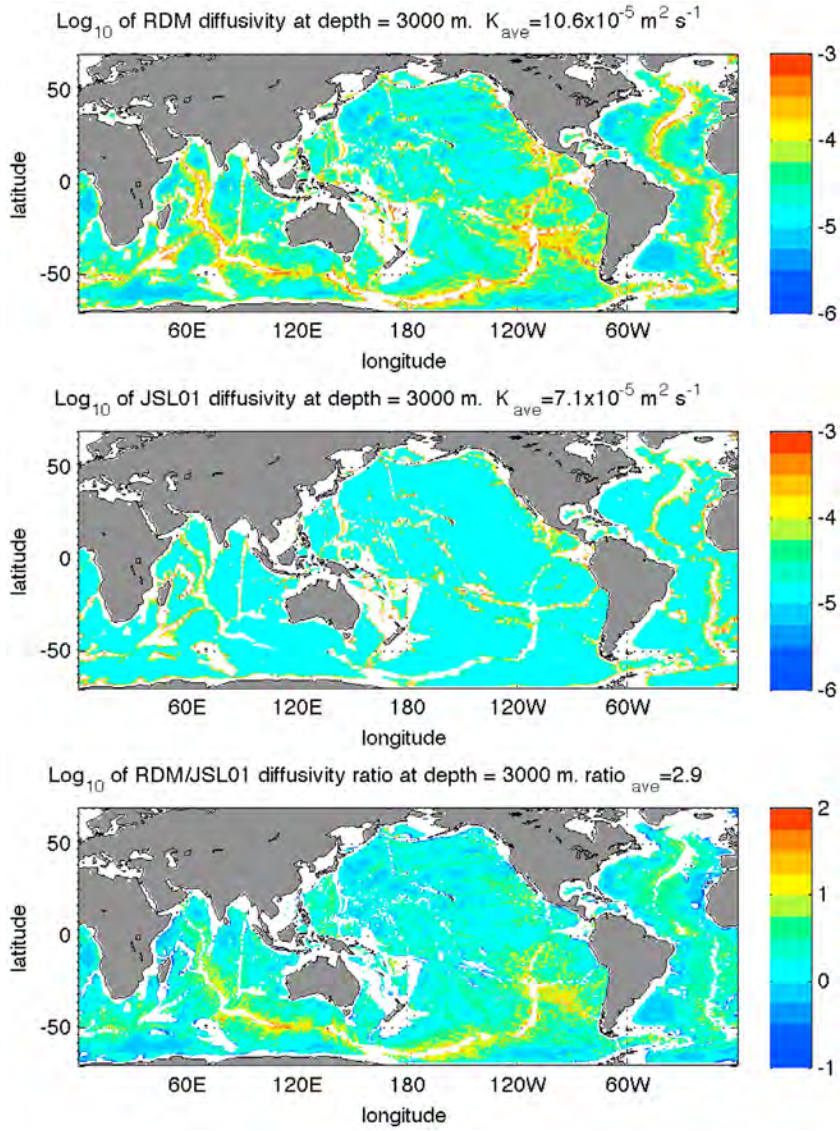

Figure 2. RDM and JSL01 diffusivities at 3000 m of depth. At the top of each frame is the averaged diffusivity at 3000 m for the entire domain (70°N-70°).

the underlying spatial distribution and should be interpreted with caution. The different spatial distributions of diffusivity by the two parameterizations would be expected to produce quite different abyssal circulation and property distributions in OGCMs.

4. Comparison of JSL01 and RDM to Inversions of WOCE Hydrography

[29] Inverse methods are routinely applied to hydrographic data in an effort to determine the mean ocean circulation consistent with observations and dynamical constraints [e.g., *Wunsch*, 1978; *Olbers et al.*, 1985; *Rintoul and Wunsch*, 1991; *Ganachaud and Wunsch*, 2000; *Ganachaud*, 2003; *Lumpkin and Speer*, 2003, 2007]. Assuming the ocean to be in steady state and geostrophic balance, hydrographic inverse models can be used to estimate mass transports and diapycnal fluxes for large ocean 'boxes' bounded by hydrographic sections and/or topography. See *Ganachaud* [2003, and references therein] for a detailed discussion of the methodology.

[30] The RDM and the JSL01 parameterizations are compared here to diapycnal diffusivity estimates by *Ganachaud* [2003] and *Lumpkin and Speer* [2007] (hereinafter referred to as GA03 and LS07). Both the GA03 and LS07 hydrographic inversions are global and based on World Ocean Circulation Experiment (WOCE) era hydrography. Both inversions compute diapycnal fluxes across neutral density surfaces (γ^n) [*Jackett and McDougall*, 1997]. The main difference between the LS07 and GA03 inversions is the explicit inclusion of air-sea fluxes in LS07, allowing estimates of transfers between outcropping layers at high latitudes. This difference is of no consequence here since we restrict the comparisons to latitudes between roughly 32°S and 48°N.

[31] Figures 4, 6, and 8 show the hydrographic sections used by GA03 and LS07 for the Pacific, Atlantic, and Indian basins. The LS07 basin-mean profiles were obtained

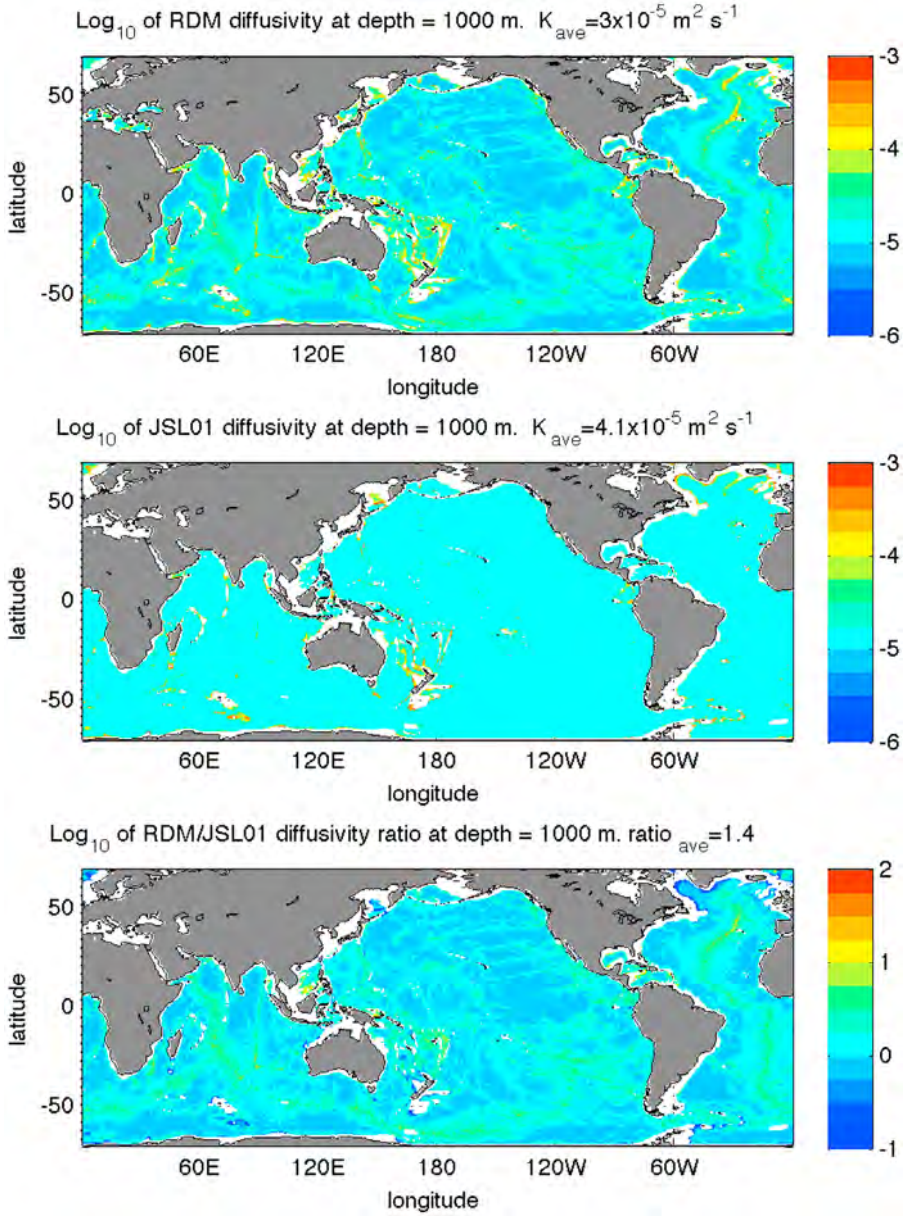

Figure 3. RDM and JSL01 diffusivities at 1000 m of depth. At the top of each frame is the averaged diffusivity at 1000 m for the entire domain (70°N-70°).

courtesy of R. Lumpkin whereas the GA03 inverse estimates are available online (http://www.pmel.noaa.gov/people/ganachaud/glbwocemodel.html). For comparison purposes, the GA03 diffusivity estimates for the smaller boxes (see Figures 4, 6, and 8) were combined into area-weighted, basin-mean averages and interpolated onto the 45 neutral density layers used by LS07. The GA03 and LS07 inversions are broadly consistent with each other, finding similar trends in the diffusivities for the different basins. In the Atlantic and Pacific midlatitude basins, the average diffusivity steadily increases with neutral density, consistent with the idea of bottom-intensified mixing and ever larger fractions being in proximity to the seafloor due to hypsometry. In the Indian Ocean, both inversions infer a remarkable averaged diffusivity close to two times greater than 10^{-4} m^2 s^{-1} over most of the water column, almost independent of depth. As noted in *St. Laurent and Simmons* [2006], the GA03 inversion generally calls for larger diffusivities than LS07. The difference is generally less than a factor of three but reaches an order of magnitude for the deepest layers in the Indian and Pacific basins. Confidence intervals reported in LS07 are the standard error whereas GA03 reports the standard deviation.

[32] We caution that considerable uncertainty is associated with diapycnal mixing inferred from inversions. This is due to both the nature of the inverse method, deducing diapycnal fluxes from small residuals between large advection by geostrophic flow [*Wunsch*, 1996], and the necessarily imperfect data sets used. The assumption that hydrographic sections are representative of the mean state of the ocean is questionable, particularly in areas of large variability such as the South Atlantic [*de Ruijter et al.*, 1999]. In addition,

Table 1a. Distribution of RDM Diffusivities at the Bottom Boundary, 3000 m and 1000 m of Depth

RDM	1000 m Depth	3000 m Depth	Bottom Boundary
$K_\rho \leq 10^{-5}$ m^2 s^{-1}	51.6%	17%	0.00%
$10^{-5} < K_\rho < 10^{-4}$ m^2 s^{-1}	45.7%	66.9%	14.3%
$10^{-4} < K_\rho < 10^{-3}$ m^2 s^{-1}	2.40%	14.4%	51.4%
$10^{-3} < K_\rho < 10^{-2}$ m^2 s^{-1}	0.30%	1.70%	34.3%
$K_\rho > 10^{-2}$ m^2 s^{-1}	0.00%	0.00%	0.00%

diapycnal fluxes (in Sv) are the primary output of the inverse models. Diapycnal diffusivities are derived quantities, based on estimates of the neutral density layer areas, and therefore dependent on the climatology used to compute the area (R. Lumpkin, personal communication, 2012). The fidelity of the inversions is therefore difficult to assess and a topic far beyond the scope of this article. Considering the scarcity of independent estimates of diapycnal mixing in the abyssal ocean, we nonetheless consider it important to compare the mixing implied by the global inversions to that of the preliminary parameterizations.

4.1. Pacific Ocean

[33] Figure 4 shows the box geometry used by GA03 and LS07 in the Pacific Ocean. Figure 5 compares the RDM and JSL01 basin-averaged (P1-P6) diapycnal diffusivity as a function of neutral density to the GA03 and LS07 inversions. As expected from section 3, the RDM and JSL01 profiles are very similar when averaged over basin scales, well within a factor of two of each other except for the deepest layers where the RDM predicts diffusivities larger than the JSL01 by a factor of 2.5. The RDM and JSL01 parameterizations are consistent with the GA03 inverse estimates up until about mid-depth, at neutral densities of $\gamma^n = 27.765$ kg m^{-3}. For deeper neutral density layers, the inversions predict diffusivities larger than the parameterizations, with a maximum difference of about a factor of 3 for the LS07, and roughly an order of magnitude for the GA03. The difference between the parameterizations and GA03 below $\gamma^n = 28.15$ kg m^{-3} is well over an order of magnitude but here the inversions themselves differ by an order of magnitude.

[34] Inspection of the smaller scale 'boxes' considered in GA03 shows that the largest differences between the inversion and the parameterizations occur in the deep Central and South Pacific. Note that the strong decrease in the LS07 diffusivities in the upper density layers of the Pacific (see Figure 5) is unphysical, likely due to the inverse model closing mass and other property budgets by erroneously projecting diapycnal transfers into air-sea fluxes of heat and freshwater (R. Lumpkin, personal communication, 2012). In the real ocean, mass and other properties in these density layers are probably balanced at least in part by diapycnal mixing.

4.2. Atlantic Ocean

[35] Figure 6 shows the hydrographic sections used in the analysis of GA03 and LS07 as well as the location of the Brazil Basin microstructure surveys. Figure 7 compares the RDM and JSL01 basin-averaged (A2–A11) diapycnal diffusivity as a function of neutral density to the GA03 and LS07 inversions. The RDM profile exceeds the JSL01 profile at all depths but they are well within a factor of two of each other, except below densities of $\gamma^n = 28.12$ kg m^{-3} where the difference reaches a factor of 5. The inversions call for diffusivities that are considerably larger than both the RDM and JSL01, although both are within the standard error of LS07's inversion. Differences range from factors of 3–5 between the RDM and LS07 and well over an order of magnitude between the JSL01 and GA03. The LS07 and (perhaps) GA03 inversions call for a maximum in the diffusivity at the $\gamma^n = 28.12$ neutral density surface, a feature reproduced by the JSL01 but not the RDM. This may reflect the deep ocean maximum in the buoyancy frequency in the western South Atlantic, a feature that would affect the JSL01 and the inversions but not the stratification-independent RDM. Inspection of the smaller scale 'boxes' considered by GA03 reveals that the central Atlantic box (A5–A9; not shown) is where the discrepancy between the parameterizations and the inverse estimate is the largest.

4.3. Indian Ocean

[36] An overview of the box geometry used by GA03 and LS07 for the Indian Ocean is shown in Figure 8. The RDM and JSL01 predicted basin-averaged profiles are compared to the inverse estimates in Figure 9. The latter infer diffusivities of nearly 2×10^{-4} m^2 s^{-1} over most of the water column, almost independent of depth. In contrast, the parameterizations predict diffusivities increasing slowly from background values near the surface reaching 1 and 3×10^{-4} m^2 s^{-1} near the bottom for the JSL01 and RDM respectively. The parameterizations yield diffusivities that are significantly smaller than diffusivities inferred from inverse estimates over most of the water column. The maximum difference between the parameterizations and LS07 is close to an order of magnitude at $\gamma^n = 27.56$ kg m^{-3}, roughly corresponding to thermocline depths. The difference between the parameterizations and GA03 is factors of 5–7 between $\gamma^n = 27.56$ and 28.12 kg m^{-3} and over an order of magnitude for deeper neutral density layers.

[37] As the youngest of the major ocean basins, the Indian Ocean is crossed by major active spreading ridges [*Stow*, 2006]. These are the Southwest Indian Ridge, the Southeast Indian and the Central Indian Ridge, joining at the Rodrigues Triple Junction and dividing the Indian Ocean into a series of deep basins. For instance, the western Indian Ocean consists of the Crozet, Madagascar, Mascarene, Somali and Arabian Basins. The Indian Ocean is further dissected between East and West by the Ninety East Ridge. The richness of topographic features suggests a strong role for topography-catalyzed, internal wave generation and mixing processes. *Drijfhout and Garabato* [2008] and

Table 1b. Distribution of JSL01 Diffusivities at the Bottom Boundary, 3000 m and 1000 m of Depth

JSL01	1000 m Depth	3000 m Depth	Bottom Boundary
$K_\rho \leq 10^{-5}$ m^2 s^{-1}	89.4%	60.6%	5.7%
$10^{-5} < K_\rho < 10^{-4}$ m^2 s^{-1}	7.80%	30.7%	49.3%
$10^{-4} < K_\rho < 10^{-3}$ m^2 s^{-1}	2.30%	7.70%	35.1%
$10^{-3} < K_\rho < 10^{-2}$ m^2 s^{-1}	0.40%	1.00%	9.40%
$K_\rho > 10^{-2}$ m^2 s^{-1}	0.03%	0.02%	0.50%

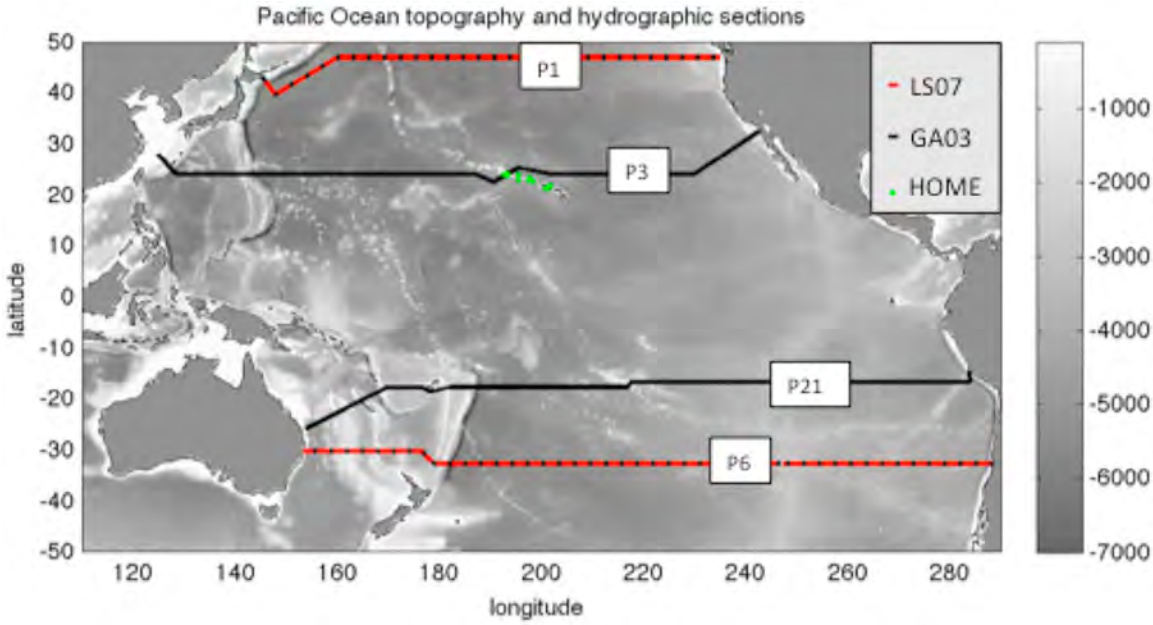

Figure 4. Pacific Ocean sections and topography. Red and black lines indicate the boundaries, respectively, of the boxes used by the LS07 and GA03 inversions considered here.

Huussen et al. [2012] provide maps illustrating the strong spatial variability of turbulent diapycnal, internal wave-driven mixing in the Indian Ocean based on the Gregg-Henyey fine-scale internal wave parameterization.

[38] In spite of the considerable internal wave-driven mixing occurring in the Indian ocean, *Huussen et al.* [2012] conclude that the diapycnal mixing required to sustain the vigorous overturning circulation inferred from hydrographic data inversions cannot be provided by internal wave breaking alone. The difference between the RDM and JSL01 parameterizations and the inverse estimates is broadly consistent with this conclusion, in the sense that these admittedly crude parameterizations of topography-catalyzed internal wave-driven mixing fall well short of the inverse estimates. This suggests the dominance of transformation processes other than breaking of topography-catalyzed internal waves. One proposal has been that the transformations occur via intense mixing in narrow passages connecting the various Indian Ocean basins. *MacKinnon et al.* [2008] infer a mean diapycnal diffusivity in excess of 10^{-2} m^2 s^{-1} several hundred meters from the bottom in the Atlantis II Fracture Zone, hypothesized to be one of the major passageways of northward flowing Circumpolar Deep Water and Antarctic Bottom Water between the Crozet and Madagascar Basins. *MacKinnon et al.* [2008] based their estimates on Thorpe scale analysis and the *Gregg et al.* [2003] fine-scale internal wave parameterization applied to LADCP/CTD measurements. *Johnson et al.* [1998] report diapycnal diffusivities of $O(10^{-4}$ m^2 s$^{-1})$ in the Amirante Passage connecting the Mascarene and Somali basins.

[39] However, the largest diffusivities inferred by the inversions are found in the Northern Indian Ocean. GA03 diffusivity estimates for the Northern Indian Ocean (north of WOCE section I2 in Figure 8) reach $8.6 \pm 4 \times 10^{-4}$ m^2 s^{-1} below the $\gamma^n = 27.36$ kg m^{-3} neutral density surface ($\sim$1000 m of depth). This is somewhat surprising given that this domain is both well north of the major bottom water passages of the southern Indian Ocean such as the Atlantis II FZ and has relatively smooth topography compared to the Southern Indian Ocean. The most prominent topographic feature in the Northern Indian Ocean is the Ninety East Ridge where *Huussen et al.* [2012] infer only weakly enhanced dissipation rates, unlike over the Southwest Indian and Central Indian Ridge where they estimate dissipation rates 2–3 orders of magnitude above background values. *Huussen et al.* [2012] attribute their inferred weak dissipation estimates to the less fractured structure of the Ninety East Ridge. Note that the Southern boundary of the North Indian Ocean box (I2-coast) crosses right over the Amirante passage, but the diffusivities observed in this passage to date [*Johnson et al.*, 1998] are much too small to account for the large basin-averaged diffusivities inferred by the hydrographic inversions.

5. Comparison of JSL01 and RDM to Microstructure Surveys

[40] *Lueck et al.* [2002] review the technological development of the use of microstructure surveys to infer TKE dissipation rate, while *Ivey et al.* [2008] provide a sobering list of fundamental issues that remain problematic in interpreting microstructure observations. Despite these concerns, microstructure surveys remain the gold standard for inferring the TKE dissipation rate. The JSL01 and RDM parameterizations are compared here to diapycnal diffusivities inferred from microstructure surveys in the Brazil Basin and around the Hawaiian Islands. A total of 165 full-depth profiles of the TKE dissipation rate were derived from High Resolution Profiler (HRP) deployments in the context of the Brazil Basin Tracer Release Experiment (BBTRE) in 1996 and 1997. The 1996 survey (BB1 hereafter) spanned nearly 30° in longitude from the relatively smooth western Brazil Basin to the rough Fracture Zones of the Mid-Atlantic Ridge

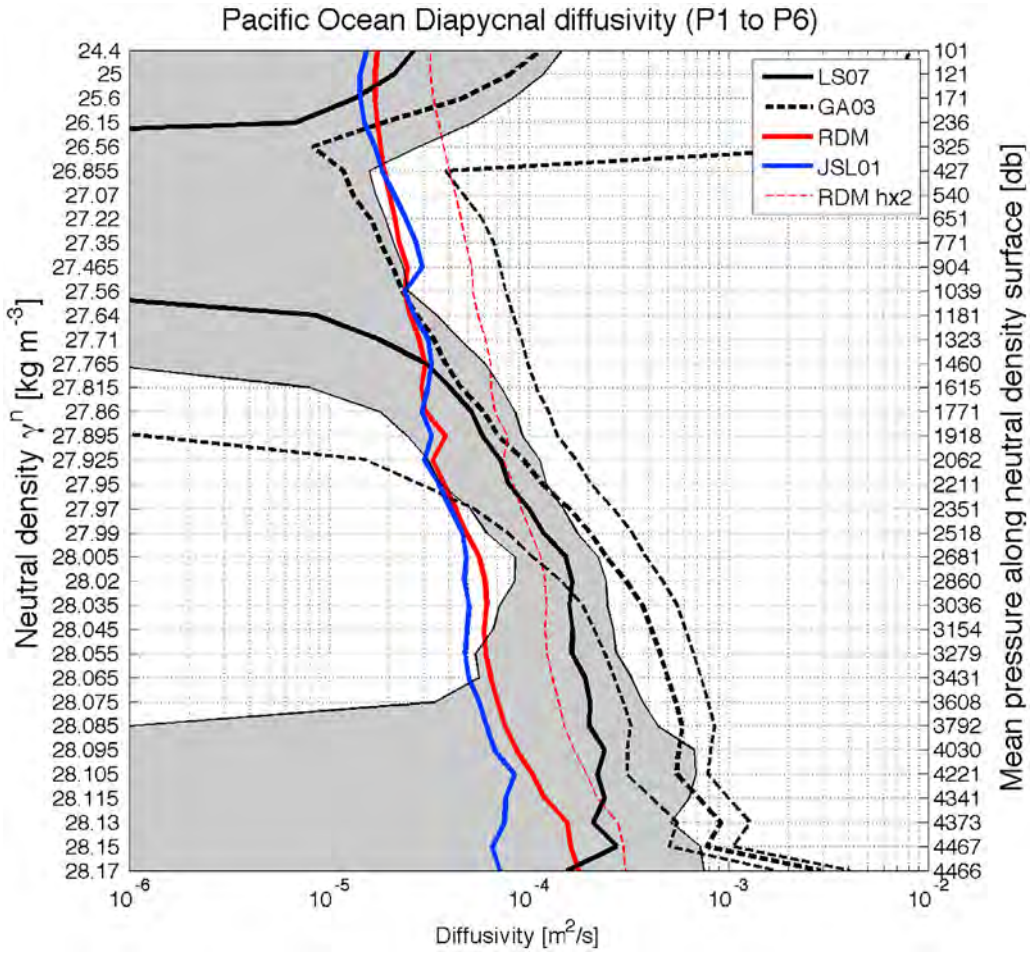

Figure 5. Pacific Ocean (P1 to P6) average diapycnal diffusivity as a function of neutral density inferred through statistical inversion of hydrography (GA03 and LS07) and predicted by the JSL01 and RDM parameterizations. The thin red dashed line represents the RDM estimate with an arbitrarily doubled scale height (see Section 7). The mean pressure along the curved neutral density surfaces is shown on the right hand side for guidance. Gray shading indicates the standard errors of the LS07 estimates, and black dashed lines indicate the standard deviations of the GA03 estimates.

whereas the 1997 survey (BB2 hereafter) was mainly conducted over the Mid-Atlantic Ridge. The HRP data was obtained courtesy of J. Toole and has been extensively analyzed previously [e.g., *Polzin et al.*, 1997; *St. Laurent et al.*, 2001; *Polzin*, 2004; *Toole*, 2007]. The microstructure data around the Hawaiian Islands was obtained from deployments of the Absolute Velocity Profiler (AVP) in the context of the Hawaiian Ocean Mixing Experiment (HOME) in 2000. The AVP was deployed around the French Frigate Shoals, Necker and Nihoa Islands and Kauai channel, yielding 13 mean TKE dissipation rate profiles. Each profile is the mean of 4 to 6 full depth AVP casts. The AVP data was obtained courtesy of J. Klymak, T. Sanford and J. Moum and has been discussed in for instance *Rudnick et al.* [2003], *Klymak et al.* [2006] and *Lee et al.* [2006].

[41] Figure 10 shows survey mean diapycnal diffusivity profiles from BBTRE and HOME as a function of height above bottom. The mean profiles were computed by first converting the individual microstructure profiles to the height above bottom coordinate system using the ocean depth measured in situ and subsequently averaging to obtain the survey mean. The 95% confidence intervals shown for 200 m height above bottom bins were computed using the bootstrap method [*Efron and Tibshirani*, 1994]. For the JSL01 and RDM, vertical diffusivity profiles are converted to functions of height above bottom based on the average depths of the 0.5° × 0.5° grid cell from the *Smith and Sandwell* [1997] global seafloor topography (v 11.1). For an interesting discussion on the issue of using coarse resolution bathymetric products to convert from depth to height above bottom, including possible misdiagnosis of the sign of diapycnal advection, the reader is referred to *Polzin* [2009].

[42] Figure 11 shows a depth-longitude section of the observed and parameterized diffusivities across the Mid-Atlantic Ridge. HRP observations are averaged in the vertical over bins centered on *Gouretski and Koltermann* [2004] climatology depth levels for comparison purposes. The HRP observations shown are a combination of BB1 and BB2 profiles chosen to maximize the zonal extent.

[43] The main feature of interest in Figures 10 and 11 is the difference in the vertical structure between the

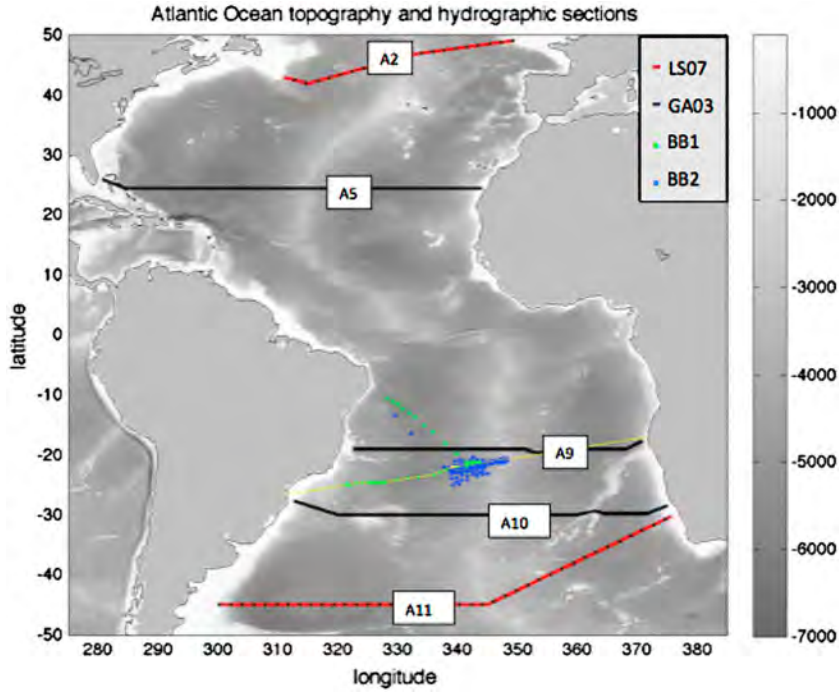

Figure 6. Atlantic Ocean sections and topography. Red and black lines indicate the boundaries, respectively, of the boxes used by the LS07 and GA03 inversions considered here. Green and blue dots indicate the locations of the 1996 and 1997 BBTRE microstructure surveys, respectively. The yellow line corresponds to the section shown in Figure 11.

observations and the parameterizations. The microstructure observations imply diffusivities well above background values up to a few kilometers off the bottom. In contrast, the JSL01 diffusivities decay close to background values within a kilometer or two from the bottom. The exception is the JSL01 prediction near the Hawaiian Ridge (Figure 10, bottom left) where JSL01 overestimates the near-boundary magnitude. The fast decay of JSL01 implies a vertical diffusivity gradient near zero much closer to topography than observed. This is particularly clear in Figure 11.

[44] Dynamically, vertical gradients of the diapycnal diffusivity dictate the strength of diapycnal advection w via the buoyancy equation [*St. Laurent*, 1999]:

$$w \approx -N^{-2}\partial_z J_b = \partial_z K_\rho + \frac{K_\rho}{N^2}\partial_z N^2 \qquad (4)$$

where $J_b = -K_\rho N^2$ is the buoyancy flux. In turn, the vertical gradient of diapycnal advection influences the geostrophic vorticity balance. That is, large-scale geostrophic flow is influenced by the second derivative of the diapycnal diffusivity with respect to the dianeutral direction. *St. Laurent et al.* [2001] present observational evidence for deep flow driven by buoyancy forcing provided by small-scale turbulent mixing in the abyssal Brazil Basin. *Saenko et al.* [2012] demonstrate numerically that the rate of the large-scale overturning can be changed by varying the scale height in the JSL01 parameterization.

[45] The RDM decay of vertical diffusivity with height above bottom fares better than the JSL01 compared to observations. The vertical dependence suggested by *Polzin* [2004] that's incorporated into the RDM is clearly a better choice than the JSL01 exponential decay with fixed scale height. The variation of the RDM scale height as a function of topographic roughness is key in allowing reasonable fits to the microstructure surveys here. However, the RDM was calibrated in part on these data sets as well as 95 microstructure profiles obtained during the 1991 Topographic Interactions Accelerated Research Initiative (TIARI) at Fieberling Guyot. Clearly, comparison to independent data sets is required to verify that a topographic roughness dependent scale height can reproduce reasonable fits at other locations, and to verify that the choice of roughness dependent scale height made for RDM is appropriate. (The data set from the narrow Fieberling Guyot was not included in Figure 10, because Fieberling is not resolved at the $0.5^\circ \times 0.5^\circ$ horizontal resolution used in this study, rendering a comparison in the height above bottom coordinate system meaningless.)

[46] In spite of being calibrated on the data sets presented here, the RDM decay is faster than observed at heights above bottom greater than 1500 m (e.g., bottom right panel of Figure 10). This may indicate the need for a scale height that varies not only in the horizontal but also in the vertical as a function of height above bottom and/or stratification. This will be considered further in Section 7.

6. Energetics

[47] *Munk* [1966] and *Munk and Wunsch* [1998] were the first to compute the power required to drive mixing in the abyssal ocean in an effort to identify the possible sources of mechanical energy. Due to crude approximations in their method, the well-known estimate of 2.1 TW for the abyssal

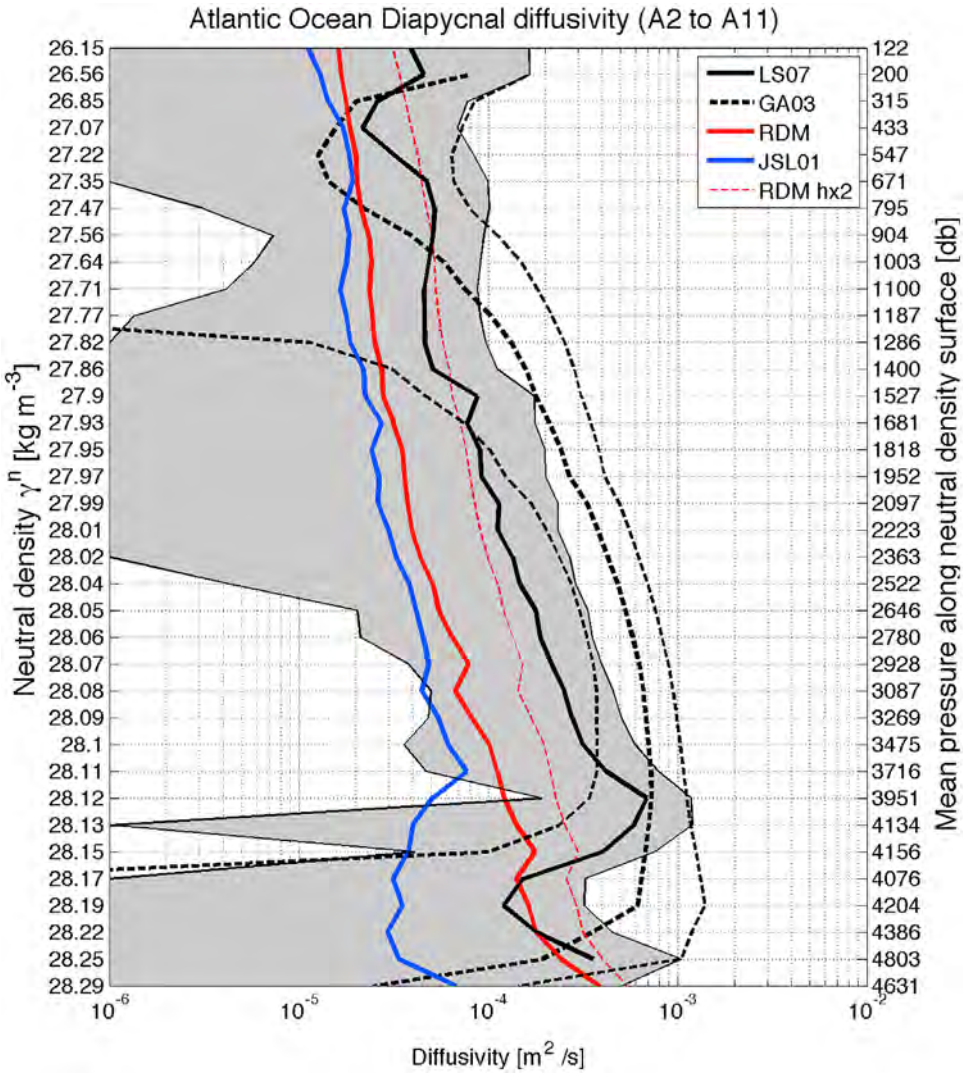

Figure 7. Atlantic Ocean (sections A11 to A2) diapycnal diffusivity as a function of neutral density inferred through statistical inversion of hydrography (GA03 and LS07) and predicted by the JSL01 and RDM parameterizations. The mean pressure along the curved neutral density surfaces is shown on the right hand side for guidance. The thin red dashed line represents the RDM estimate with an arbitrarily doubled scale height (see Section 7). Confidence intervals as in Figure 5.

ocean volume (1–4 km depth, 48°N and 32°S) associated with a constant diffusivity of 10^{-4} m^2 s^{-1} is likely high by a factor of 3 [*Decloedt and Luther*, 2010; *Klocker and McDougall*, 2010]. Table 2 summarizes the power consumed by the JSL01 and RDM parameterizations and the hydrographic inversions below 1 km of depth and latitudinally restricted between the hydrographic lines used for the inversions, roughly encompassing the global ocean between 48°N and 32°S. The power consumption is computed [e.g., *St. Laurent and Simmons*, 2006] as

$$P = (1 + 1/\Gamma) \int \rho K_\rho(x,y,z) N^2(x,y,z) dV \qquad (5)$$

where Γ is the mixing efficiency and N is the buoyancy frequency. $N(x, y, z)$ is computed from the *Gouretski and Koltermann* [2004] climatology. *Munk and Wunsch* [1998] integrated the oceanic buoyancy assuming $\int N^2(x, y, z) dV \approx A \int N^2(z) dz \approx Ag\Delta\rho$ where A is the area of the ocean, g is the acceleration due to gravity, and the density difference $\Delta\rho$ between 1 and 4 km of depth roughly approximated as 1 kg m^{-3}.]

[48] Globally, abyssal power consumption estimates range from ~0.3 TW for JSL01 to 1.6 TW for the GA03 inverse estimates. Current best estimates of the mechanical energy available for diapycnal mixing in the abyssal ocean are ~2 TW [e.g., *Wunsch and Ferrari*, 2004]. As discussed in section 2.1, it is likely that a sizable fraction of this potentially available mechanical energy is dissipated in the upper ocean. The power requirement for diapycnal mixing in the abyssal ocean should therefore be less than 2 TW on energetic grounds alone. We hence consider the GA03 1.6 TW estimate to be on the high side, since this would require almost all of the mechanical energy potentially available to be consumed by diapycnal mixing. The JSL01, RDM and

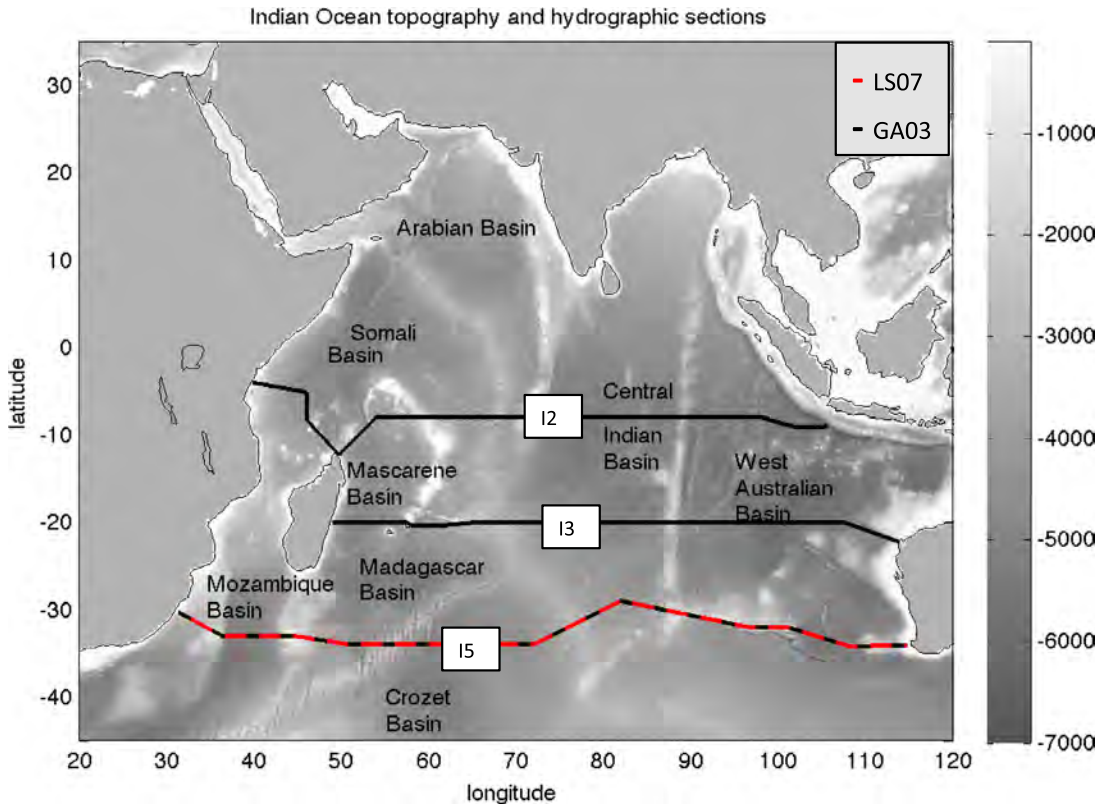

Figure 8. Indian Ocean sections and topography. Red and black lines indicate the boundaries, respectively, of the boxes used by the LS07 and GA03 inversions considered here. Major basins referred to in the text are marked.

LS07 estimates are below 1 TW each, and are more readily reconciled with current estimates of mechanical energy available in the abyssal ocean. Geographically, power consumption in the Atlantic and Indian Ocean basins are of comparable magnitude to each other for all the estimates. By virtue of its vast volume, the Pacific generally consumes by far the most power, except for the LS07 estimates due to its strong, unphysical decrease in the effective diffusivity in the upper density layers of the Pacific (see Figure 5) leading to weaker than expected power consumption.

[49] As discussed in *Decloedt and Luther* [2010], power consumption estimates are sensitive to the spatial variability of both the diapycnal diffusivity and the stratification. Especially, it was found that power estimates based on basin-averaged diffusivities were biased high compared to estimates based on using the actual spatial distribution of the diffusivities in (4). This is because, as noted in section 3, averages of spatially varying diffusivities are themselves biased high due to the quasi-lognormal distribution typical of turbulence parameters in the ocean. Therefore, the power consumption estimates associated with the inverse estimates can be expected to be upper limits.

7. Discussion and Conclusions

[50] In the past decade, numerous OGCM sensitivity studies have demonstrated that it is important to accurately parameterize both the geographical distribution and vertical structure of diapycnal mixing in the abyssal ocean in order to improve the verisimilitude of OGCM simulations. Existing spatially varying mixing parameterizations remain rudimentary and have been subjected to little validation. In this paper, two preliminary parameterizations differing significantly in their conceptual approaches are compared to available microstructure surveys and global hydrographic inversions in an effort to guide future improvements to parameterizations. The JSL01 focuses on the local dissipation of internal tides, prescribing bottom-intensified mixing only in regions of combined barotropic tidal forcing and topographic roughness whereas the RDM prescribes bottom-intensified mixing over all rough topography. The JSL01 and RDM can be viewed as approximations to total, topography-catalyzed, internal wave driven mixing in the abyssal ocean, the JSL01 being conservative and the RDM liberal respectively. As discussed in section 3, the resulting horizontal distributions are significantly different, in particular in the Southern Hemisphere.

[51] In spite of the significantly different horizontal distributions, the JSL01 and RDM basin-averaged diapycnal diffusivity profiles are remarkably similar, generally differing by less than a factor of two at most depths. Both are consistently conservative (smaller diffusivities) compared to basin-scale hydrographic inversions. Little can therefore be said about the validity of either geographical distribution by comparing the basin-averaged profiles to the inversions, pointing to the need for more microstructure surveys for validation purposes.

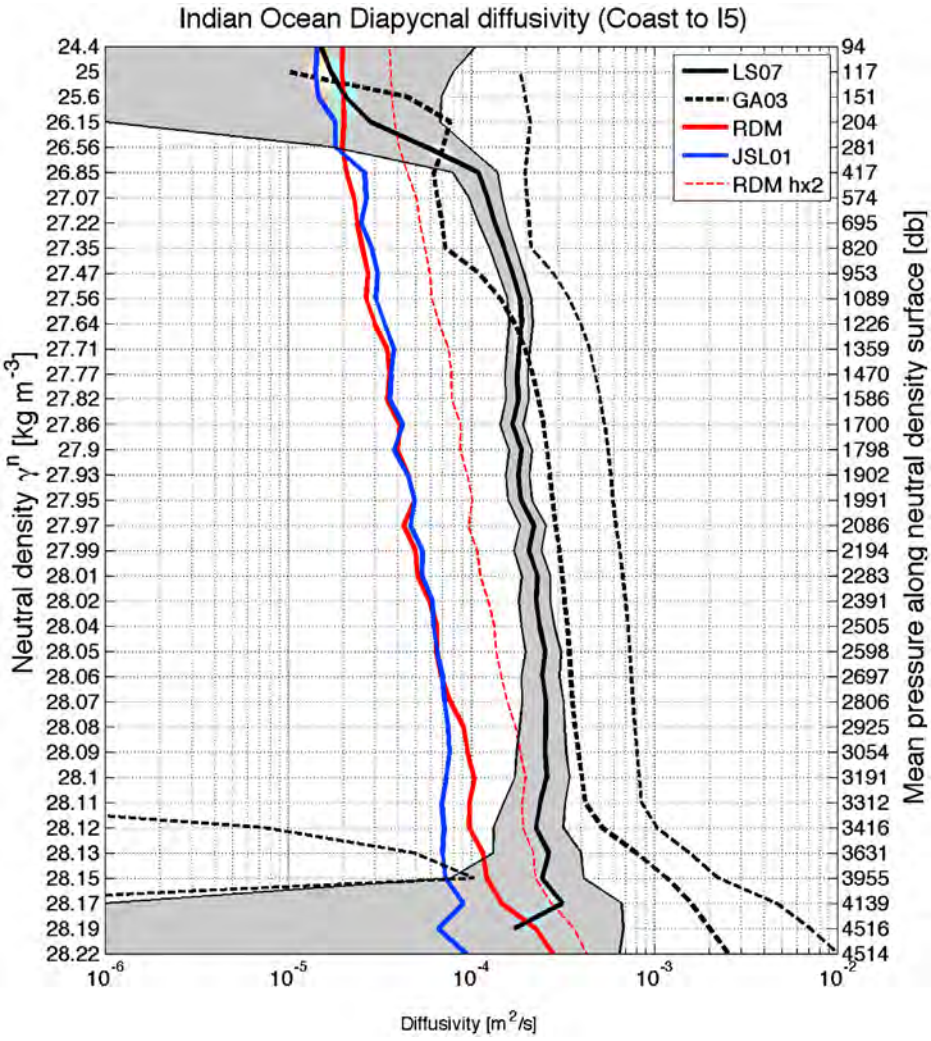

Figure 9. Indian Ocean (I5 to coast) diapycnal diffusivity as a function of neutral density inferred through statistical inversion of hydrography (GA03 and LS07) and predicted by the JSL01 and RDM parameterizations. The mean pressure along the curved neutral density surfaces is shown on the right hand side for guidance. The thin red dashed line represents the RDM estimate with an arbitrarily doubled scale height (see Section 7). Confidence intervals as in Figure 5.

[52] Assuming the LS07 and GA03 inverse estimates yield realistic profiles of the diapycnal diffusivity, both the JSL01 and RDM parameterizations significantly underestimate mixing in the abyssal ocean, often by as much as an order of magnitude. Comparisons to microstructure surveys imply that bottom-intensified mixing also extends further into the water column than either parameterization predicts. This discrepancy is likely due to oversimplified vertical structure functions. While the RDM's power law approach with a horizontally varying scale height and boundary intensity [cf. *Iwamae and Hibiya*, 2012] certainly is an improvement over the exponential decay with constant scale height used in JSL01 (e.g., Figure 10), the results here suggest that the scale height should also vary in the vertical to take into account a weakening of the wave-wave interactions with distance from bottom and variable stratification effects.

[53] A vertical variation of the scale height is consistent with the theoretical framework developed by *Polzin* [2004, 2009], linking the turbulent dissipation to the decay of the internal wavefield via nonlinear wave-wave interactions. Internal wave generation over rough topography energizes the near-boundary internal wavefield, as evidenced for instance in observations of enhanced fine scale shear and strain spectral levels [e.g., *Polzin et al.*, 1997; *Toole et al.*, 1997]. Nonlinear wave-wave interactions are expected to transport energy down to smaller vertical scales where shear instability takes place, ultimately leading to turbulent dissipation [*Toole*, 1998]. The efficiency of wave-wave interactions is associated with shear spectral levels [*Polzin et al.*, 1995]. The turbulent dissipation rate at a given height above bottom is therefore a function of the available energy (shear spectral amplitude) and the efficiency at which the energy is cascaded to dissipation scales (strength of wave-wave interactions). With increasing height above bottom, an increasing fraction of energy has been dissipated, implying a decay of the spectral amplitude and therefore also less efficient wave-wave interactions. The turbulent dissipation rate therefore decays with height above bottom since both the

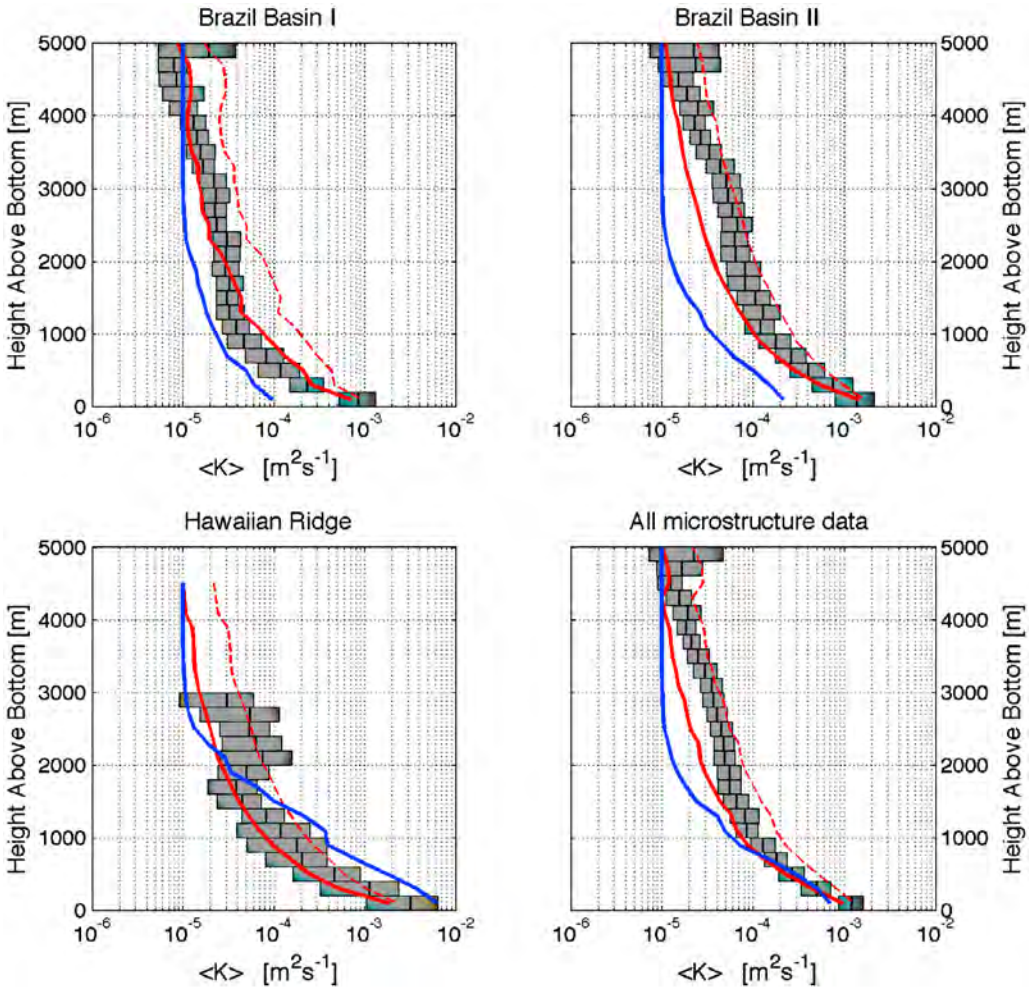

Figure 10. Survey averaged diapycnal diffusivity profiles as a function of height above bottom for the 1996 (Brazil Basin 1) and 1997 (Brazil Basin 2) BBTRE HRP microstructure surveys and the AVP HOME microstructure survey around the Hawaiian Ridge. Observations are binned in 200 m height-above-bottom bins. 95% bootstrapped confidence intervals are shown in gray. The red (blue) curves are the averages of the RDM (JSL01) predictions made at each observed profile site. The thin red dashed line represents the RDM estimate with an arbitrarily doubled scale height (see Section 7).

spectral amplitude and the efficiency of wave-wave interactions weaken. Furthermore, since both the spectral amplitude and strength of wave-wave interactions generally decrease in concert with height above bottom, the relative decay of the spectrum gradually slows down. In terms of scale height h_0 in (3) specifying the vertical structure of ε, the scale height increases with height above bottom.

[54] The scale height also depends on the ambient stratification. *Polzin* [2004, 2009] argues that the high vertical wave number spectral density varies in proportion to N^2. The effect of this buoyancy scaling is to influence the efficiency of the energy transport toward smaller scales via wave-wave interactions, even at constant spectral amplitude. In the case of waves propagating into increasing stratification, the efficiency of the energy transport toward smaller scales via wave-wave interactions increases, implying an increase in TKE dissipation rates compared to the case of constant stratification.

[55] A fixed scale height at a given location can thus not be expected to capture both the near-boundary vertical structure and the decay far off the bottom. We speculate that the combination of both large distance from the bottom and variable stratification is the cause of the discrepancy between observed and RDM diffusivities as seen for instance in Figure 10 at heights above bottom greater than ~1500 m. First, at those distances from the bottom, the scale height should be larger than at the bottom, implying slower relative decay of the dissipation rate than modeled by the RDM. Second, at those heights above bottom, the bottom-generated internal waves reach thermocline levels where stratification strengthens considerably, leading to more efficient wave-wave interactions and thus stronger dissipation rates. The relative importance of either effect requires further study.

[56] As a crude test to see whether the discrepancy between the inferred and parameterized basin-averaged profiles can be explained by the faster than observed vertical decay in the parameterizations, the RDM scale height was doubled. This leaves the boundary value unchanged but leads to higher diffusivities compared to the microstructure

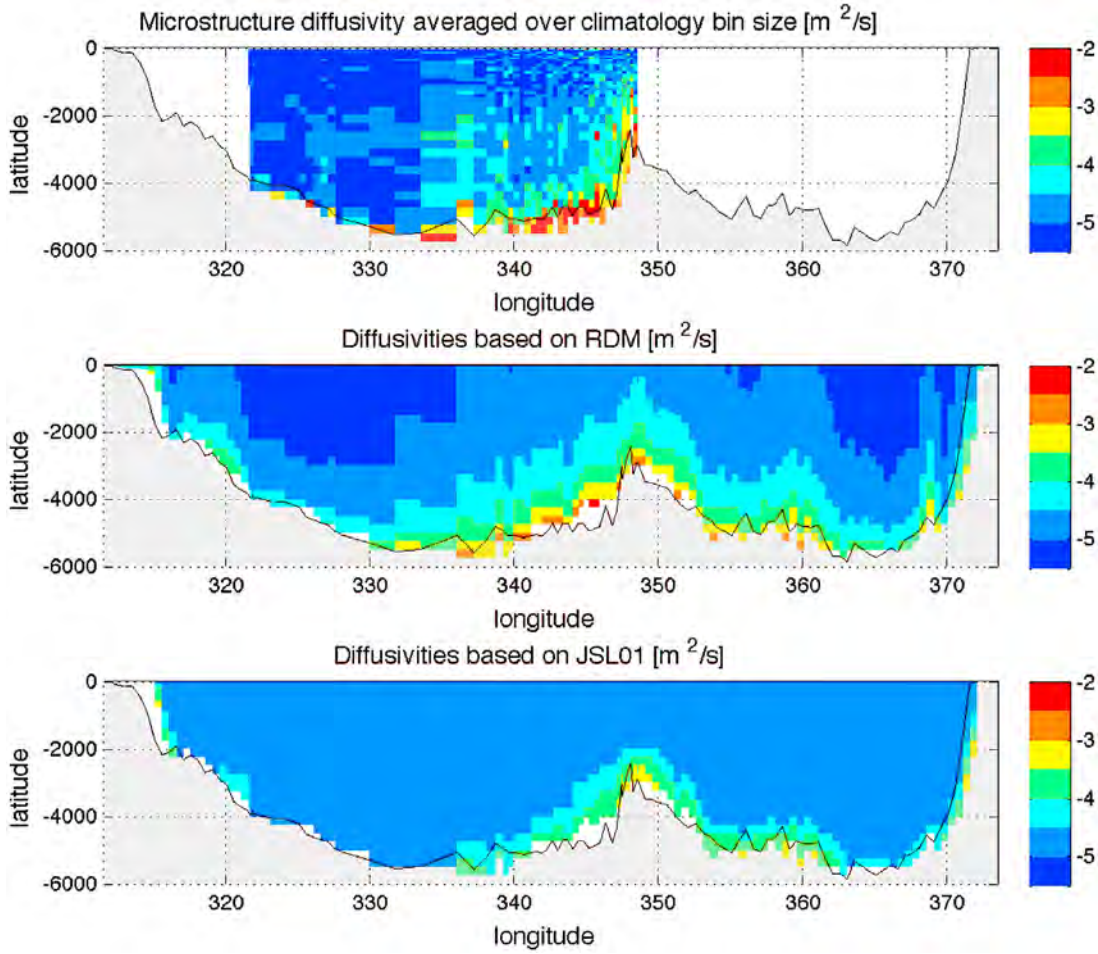

Figure 11. Depth-longitude plots of diffusivities across the mid-Atlantic Ridge as (top) inferred from the HRP profiler in the Brazil Basin (observations sites shown in Figure 6) and predicted by the (middle) RDM and (bottom) JSL01 parameterizations. HRP observations are averaged over bins centered on *Gouretski and Koltermann* [2004] climatology depth levels for comparison purposes. The topography shown is based on the *Smith and Sandwell* [1997] v11.1 bathymetry.

data in the first 2000 m above bottom and marginally higher or consistent diffusivities compared with the microstructure data higher up in the water column (thin dashed red line in Figure 10). The slower decay has a significant effect on basin-averaged diffusivities, generally doubling their values, but they are still conservative compared to the inverse estimates in the abyssal ocean (thin dashed red lines, Figures 5, 7, and 9).

[57] Assuming the inversions are realistic, the implication is that more abyssal water mass transformations are occurring than can be mimicked by improvements to the vertical structure functions in the current parameterizations based on concepts of internal wave induced mixing. This might indicate that the RDM and JSL01 parameterizations are too conservative in estimating the maximum boundary diffusivities, or that abyssal mixing processes other than breaking of bottom-generated internal waves are at play. Comparison of the smaller scale boxes analyzed by GA03 with the parameterizations yields some evidence for the latter since regions where the inversions differ most from the parameterizations are often locations where intense mixing through constricted passages has been inferred. In the North Tropical Atlantic, intense mixing in the Vema and Romanche Fracture Zones is well documented. The Vema Fracture Zone, with a sill depth of more than 4500 m of depth, allows transport of Antarctic Bottom Water (AABW) from the Western to the Eastern Atlantic. The observed isopycnal field is consistent with an internal hydraulic jump, with overturns as large as 400 m having been inferred [*Mauritzen and Polzin*, 2003]. Intense mixing is also documented in the Romanche Fracture Zone [*Polzin et al.*, 1996; *Ferron et al.*, 1998]. *Ferron et al.* [1998] report a mean diapycnal diffusivity of 10^{-1} m^2 s^{-1}, and strong mixing up to 1000 m above the bottom at the northern exit. *Polzin* [1996] suggests flow within the Romanche Fracture Zone is hydraulically controlled. Likewise, intense, $O(10^{-1}$ m^2 s$^{-1})$, mixing occurring in the Samoan Passage [*Roemmich et al.*, 1996] may contribute to the discrepancy between the parameterizations and the hydrographic inversions in the deep Pacific.

[58] In the Indian Ocean Basin where the discrepancy between inversions and parameterizations is the most severe, intense mixing at the various passages connecting the deep

Table 2. Power Consumption by Diapycnal Mixing Below 1 km of Depth, Between Roughly 32°S and 48°N, for the RDM and JSL01 Parameterizations and the GA03 and LS07 Inverse Estimates[a]

	GA03	LS07	RDM	JSL01
Atlantic Ocean				
A2–A5	16 GW	52 GW	22 GW	14 GW
A5–A9	298 GW	108 GW	55 GW	25 GW
A9–A10	163 GW	32 GW	15 GW	8 GW
A10–A11	8 GW	41 GW	19 GW	11 GW
Atlantic total	0.48 TW	0.23 TW	0.11 TW	0.06 TW
Indian Ocean				
North of I2	384 GW	112 GW	32 GW	29 GW
I2–I3	25 GW	74 GW	19 GW	21 GW
I3–I5	67 GW	100 GW	29 GW	21 GW
Indian total	0.48 TW	0.29 TW	0.08 TW	0.07 TW
Pacific Ocean				
P1–P3	51 GW	47 GW	22 GW	25 GW
P3–P21	355 GW	151 GW	139 GW	100 GW
P21–P6	238 GW	43 GW	46 GW	30 GW
Pacific total	0.64 TW	0.24 TW	0.21 TW	0.15 TW
Global total	1.60 TW	0.76 TW	0.40 TW	0.28 TW

[a]For the GA03 estimates, a diffusivity profile for each ocean volume delineated by the hydrographic sections noted below was available and used for the estimates. For LS07, only a single vertically averaged diffusivity profile per basin was available. The fully spatially varying diffusivity fields were used for the RDM and JSL01 estimates.

Basins may be partly responsible. Indeed, many observational studies infer strong diapycnal mixing rates in passageways between deep Indian Ocean basins [e.g., *Johnson et al.*, 1998; *MacKinnon et al.*, 2008]. But mixing in these deep passages is at best only a partial explanation for the large discrepancies between diffusivity estimates from hydrographic inversions and the diffusivity parameterizations (Figures 5, 7, and 9), because the mixing action is confined to the deepest oceanic layers yet the discrepancies are large up into the thermocline. As pointed out by *St. Laurent and Thurnherr* [2007], most of the above work targets prominent passages and fracture zones. Their work on the Lucky Strike passage, a small passage below the resolution of satellite bathymetry on the mid-Atlantic Ridge crest, suggests that turbulence resulting from flow through the many thousands of such narrow passages existing on the global mid-ocean ridges may cumulatively equate to buoyancy fluxes equivalent to those of the major passages and fracture zones, and, because these sites are at shallower depths, influence mixing rates up to the base of the thermocline.

[59] In summary, the results here indicate that preliminary, spatially heterogeneous mixing parameterizations such as JSL01 and RDM are conservative in both the magnitude of total abyssal mixing implied, and the vertical extent to which they allow bottom-intensified mixing to penetrate into the water column. Comparison with microstructure surveys suggests the latter issue can be addressed by improving vertical structure functions, such as the stratification-dependent scale height approach formulated by *Polzin* [2009]. A more serious issue may be the significant discrepancy between the basin-scale inversions and the preliminary parameterizations. Assuming the inversions are realistic, a plausible interpretation is that parameterizing topography-catalyzed, internal wave driven mixing is not sufficient to approximate the spatial distribution of total diapycnal mixing in the abyssal ocean. The current trend in improving mixing parameterizations is to combine maps of energy conversion of, for instance, tidal and eddy dissipation as was recently done in *Saenko et al.* [2012]. This approach, especially if coupled with improved vertical structure functions, might well improve the comparison with the inversions, but the results here indicate that separate parameterizations targeting mixing localized in canyons and narrow passageways will probably need to be added to improve comparisons with the inversions. The fidelity of the inversions is a topic far beyond the scope of this article and will not be discussed.

[60] **Acknowledgments.** We gratefully acknowledge A. Ganachaud, S. Jayne, J. Klymak, R. Lumpkin, J. Moum, T. Sanford and J. Toole for kindly sharing their data. This work was made possible by National Science Foundation Grant OCE-0961262.

References

Alford, M. H. (2003), Improved global maps and 54-year history of windwork on ocean inertial motions, *Geophys. Res. Lett.*, *30*(8), 1424, doi:10.1029/2002GL016614.

Alford, M. H., J. A. MacKinnon, Z. X. Zhao, R. Pinkel, J. Klymak, and T. Peacock (2007), Internal waves across the Pacific, *Geophys. Res. Lett.*, *34*, L24601, doi:10.1029/2007GL031566.

Althaus, A. M., E. Kunze, and T. B. Sanford (2003), Internal tide radiation from Mendocino Escarpment, *J. Phys. Oceanogr.*, *33*, 1510–1527, doi:10.1175/1520-0485(2003)033<1510:ITRFME>2.0.CO;2.

Ascani, F., E. Firing, P. Dutrieux, J. McCreary, and A. Ishida (2010), Deep equatorial ocean circulation induced by a forced-dissipated Yanai beam, *J. Phys. Oceanogr.*, *40*, 1118–1142, doi:10.1175/2010JPO4356.1.

Aucan, J., M. A. Merrifield, D. S. Luther, and P. Flament (2006), Tidal mixing events on the deep flanks of Kaena Ridge, Hawaii, *J. Phys. Oceanogr.*, *36*, 1202–1219, doi:10.1175/JPO2888.1.

Bell, T. (1975), Lee waves in stratified flows with simple harmonic time dependence, *J. Fluid Mech.*, *67*, 705–722, doi:10.1017/S0022112075000560.

Bryan, F. (1987), Parameter sensitivity of primitive equation ocean general-circulation models, *J. Phys. Oceanogr.*, *17*, 970–985, doi:10.1175/1520-0485(1987)017<0970:PSOPEO>2.0.CO;2.

Bryan, K., and L. Lewis (1979), A water mass model of the world ocean, *J. Geophys. Res.*, *84*, 2503–2517, doi:10.1029/JC084iC05p02503.

Carter, G. S., and M. C. Gregg (2002), Intense, variable mixing near the head of Monterey Submarine Canyon, *J. Phys. Oceanogr.*, *32*, 3145–3165, doi:10.1175/1520-0485(2002)032<3145:IVMNTH>2.0.CO;2.

Carter, G. S., M. C. Gregg, and M. A. Merrifield (2006), Flow and mixing around a small seamount on Kaena Ridge, Hawaii, *J. Phys. Oceanogr.*, *36*, 1036–1052, doi:10.1175/JPO2924.1.

Danioux, E., P. Klein, and P. Riviere (2008), Propagation of wind energy into the deep ocean through a fully turbulent mesoscale eddy field, *J. Phys. Oceanogr.*, *38*, 2224–2241, doi:10.1175/2008JPO3821.1.

Decloedt, T., and D. S. Luther (2010), On a simple empirical parameterization of topography-catalyzed diapycnal mixing in the abyssal ocean, *J. Phys. Oceanogr.*, *40*, 487–508, doi:10.1175/2009JPO4275.1.

de Ruijter, W. P. M., A. Biastoch, S. S. Drijfhout, J. R. E. Lutjeharms, R. P. Matano, T. Pichevin, P. J. van Leeuwen, and W. Weijer (1999), Indian-Atlantic interocean exchange: Dynamics, estimation and impact, *J. Geophys. Res.*, *104*(C9), 20,885–20,910, doi:10.1029/1998JC900099.

Drijfhout, S. S., and A. C. N. Garabato (2008), The zonal dimension of the Indian Ocean meridional overturning circulation, *J. Phys. Oceanogr.*, *38*, 359–379.

Duteil, O., and A. Oschlies (2011), Sensitivity of simulated extent and future evolution of marine suboxia to mixing intensity, *Geophys. Res. Lett.*, *38*, L06607, doi:10.1029/2011GL046877.

Efron, B., and R. J. Tibshirani (1994), *An Introduction to the Bootstrap*, Chapman and Hall, New York.

Egbert, G. D., and R. D. Ray (2000), Significant dissipation of tidal energy in the deep ocean inferred from satellite altimeter data, *Nature*, *405*, 775–778, doi:10.1038/35015531.

Ferrari, R., and D. Ferreira (2011), What processes drive the ocean heat transport?, *Ocean Modell.*, *38*, 171–186, doi:10.1016/j.ocemod.2011.02.013.

Ferron, B., H. Mercier, K. Speer, A. Gargett, and K. Polzin (1998), Mixing in the Romanche Fracture Zone, *J. Phys. Oceanogr.*, *28*, 1929–1945, doi:10.1175/1520-0485(1998)028<1929:MITRFZ>2.0.CO;2.

Friedrich, T., A. Timmermann, T. Decloedt, D. S. Luther, and A. Mouchet (2011), The effect of topography-enhanced diapycnal mixing on ocean and atmospheric circulation and marine biogeochemistry, *Ocean Modell.*, *39*, 262–274, doi:10.1016/j.ocemod.2011.04.012.

Fu, L. L., T. Keffer, P. P. Niiler, and C. Wunsch (1982), Observations of mesoscale variability in the western North Atlantic: A comparative study, *J. Mar. Res.*, *40*, 809–848.

Furuichi, N., T. Hibiya, and Y. Niwa (2008), Model-predicted distribution of wind-induced internal wave energy in the world's oceans, *J. Geophys. Res.*, *113*, C09034, doi:10.1029/2008JC004768.

Ganachaud, A. (2003), Large-scale mass transports, water mass formation, and diffusivities estimated from World Ocean Circulation Experiment (WOCE) hydrographic data, *J. Geophys. Res.*, *108*(C7), 3213, doi:10.1029/2002JC001565.

Ganachaud, A., and C. Wunsch (2000), Improved estimates of global ocean circulation, heat transport and mixing from hydrographic data, *Nature*, *408*, 453–457, doi:10.1038/35044048.

Garabato, A. C. N., D. P. Stevens, and K. J. Heywood (2003), Water mass conversion, fluxes, and mixing in the Scotia Sea diagnosed by an inverse model, *J. Phys. Oceanogr.*, *33*, 2565–2587.

Garrett, C., and W. H. Munk (1972), Space time scales of internal waves, *Geophys. Fluid Dyn.*, *2*, 291–297.

Gille, S. T., M. M. Yale, and D. T. Sandwell (2000), Global correlation of mesoscale ocean variability with seafloor roughness from satellite altimetry, *Geophys. Res. Lett.*, *27*, 1251–1254, doi:10.1029/1999GL007003.

Goff, J. A., and B. K. Arbic (2010), Global prediction of abyssal hill roughness statistics for use in ocean models from digital maps of paleo-spreading rate, paleo-ridge orientation, and sediment thickness, *Ocean Modell.*, *32*, 36–43, doi:10.1016/j.ocemod.2009.10.001.

Goff, J., and T. Jordan (1988), Stochastic modelling of seafloor morphology: Inversion of sea beam data for second-order statistics, *J. Geophys. Res.*, *93*, 13,589–13,608, doi:10.1029/JB093iB11p13589.

Goosse, H., et al. (2010), Description of the Earth system model of intermediate complexity LOVECLIM version 1.2, *Geosci. Model Dev.*, *3*, 603–633, doi:10.5194/gmd-3-603-2010.

Gouretski, V., and K. Koltermann (2004), WOCE global hydrographic climatology, *Tech. Rep. 35*, 49 pp., Bundesamtes für Seeschiffahrt und Hydrogr., Hamburg, Germany.

Green, J. A. M., C. L. Green, G. R. Bigg, T. P. Rippeth, J. D. Scourse, and K. Uehara (2009), Tidal mixing and the Meridional Overturning Circulation from the Last Glacial Maximum, *Geophys. Res. Lett.*, *36*, L15603, doi:10.1029/2009GL039309.

Gregg, M. C. (1987), Diapycnal mixing in the thermocline: A review, *J. Geophys. Res.*, *92*, 5249–5286, doi:10.1029/JC092iC05p05249.

Gregg, M. C., T. B. Sanford, and D. P. Winkel (2003), Reduced mixing from the breaking of internal waves in equatorial waters, *Nature*, *422*, 513–515, doi:10.1038/nature01507.

Guiles, M. (2009), Energy redistribution through tidal and inertial wave interaction, PhD dissertation, Dep. of Oceanogr., Univ. of Hawai'i at Mānoa, Honolulu.

Harrison, M., and R. Hallberg (2008), Pacific subtropical cell response to reduced equatorial dissipation, *J. Phys. Oceanogr.*, *38*, 1894–1912, doi:10.1175/2008JPO3708.1.

Henyey, F., J. Wright, and S. Flatte (1986), Energy and action flow through the internal wave field: An eikonal approach, *J. Geophys. Res.*, *91*, 8487–8495, doi:10.1029/JC091iC07p08487.

Hibiya, T., M. Nagasawa, and Y. Niwa (2002), Nonlinear energy transfer within the oceanic internal wave spectrum at mid and high latitudes, *J. Geophys. Res.*, *107*(C11), 3207, doi:10.1029/2001JC001210.

Hibiya, T., M. Nagasawa, and Y. Niwa (2006), Global mapping of diapycnal diffusivity in the deep ocean based on the results of expendable current profiler (XCP) surveys, *Geophys. Res. Lett.*, *33*, L03611, doi:10.1029/2005GL025218.

Huang, R. X., and X. Z. Jin (2002), Deep circulation in the South Atlantic induced by bottom-intensified mixing over the midocean ridge, *J. Phys. Oceanogr.*, *32*, 1150–1164, doi:10.1175/1520-0485(2002)032<1150:DCITSA>2.0.CO;2.

Hughes, C. W., and C. Wilson (2008), Wind work on the geostrophic ocean circulation: An observational study of the effect of small scales in the wind stress, *J. Geophys. Res.*, *113*, C02016, doi:10.1029/2007JC004371.

Huussen, T., A. C. Naveira-Garabato, H. Bryden, and E. McDonagh (2012), Is the deep Indian Ocean MOC sustained by breaking internal waves?, *J. Geophys. Res.*, *117*, C08024, doi:10.1029/2012JC008236.

Ivey, G. N., K. B. Winters, and J. R. Koseff (2008), Density stratification, turbulence but how much mixing?, *Annu. Rev. Fluid Mech.*, *40*, 169–184, doi:10.1146/annurev.fluid.39.050905.110314.

Iwamae, N., and T. Hibiya (2012), Numerical study of tide-induced mixing over rough bathymetry in the abyssal ocean, *J. Oceanogr.*, *68*, 195–203, doi:10.1007/s10872-011-0088-2.

Jackett, D. R., and T. J. McDougall (1997), A neutral density variable for the world's oceans, *J. Phys. Oceanogr.*, *27*, 237–263, doi:10.1175/1520-0485(1997)027<0237:ANDVFT>2.0.CO;2.

Jayne, S. R. (2009), The impact of abyssal mixing parameterizations in an ocean general circulation model, *J. Phys. Oceanogr.*, *39*, 1756–1775, doi:10.1175/2009JPO4085.1.

Jayne, S. R., and L. C. St. Laurent (2001), Parameterizing tidal dissipation over rough topography, *Geophys. Res. Lett.*, *28*, 811–814, doi:10.1029/2000GL012044.

Jing, Z., L. Wu, L. Li, C. Liu, X. Liang, Z. Chen, D. Hu, and Q. Liu (2011), Turbulent diapycnal mixing in the subtropical northwestern Pacific: Spatial-seasonal variations and role of eddies, *J. Geophys. Res.*, *116*, C10028, doi:10.1029/2011JC007142.

Jochum, M. (2009), Impact of latitudinal variations in vertical diffusivity on climate simulations, *J. Geophys. Res.*, *114*, C01010, doi:10.1029/2008JC005030.

Johnson, G. C., D. L. Musgrave, B. A. Warren, A. Ffield, and D. B. Olson (1998), Flow of bottom and deep water in the Amirante Passage and Mascarene Basin, *J. Geophys. Res.*, *103*, 30,973–30,984, doi:10.1029/1998JC900027.

Johnston, T. M. S., and M. A. Merrifield (2003) Internal tide scattering at seamounts, ridges, and islands, *J. Geophys. Res.*, *108*(C6), 3180, doi:10.1029/2002JC001528.

Katsman, C. A. (2006), Impacts of localized mixing and topography on the stationary abyssal circulation, *J. Phys. Oceanogr.*, *36*, 1660–1671, doi:10.1175/JPO2925.1.

Klocker, A., and T. McDougall (2010), Influence of the nonlinear equation of state on global estimates of dianeutral advection and diffusion, *J. Phys. Oceanogr.*, *40*, 1690–1709, doi:10.1175/2010JPO4303.1.

Klymak, J. M., J. N. Moum, J. D. Nash, E. Kunze, J. B. Girton, G. S. Carter, C. M. Lee, T. B. Sanford, and M. C. Gregg (2006), An estimate of tidal energy lost to turbulence at the Hawaiian Ridge, *J. Phys. Oceanogr.*, *36*, 1148–1164, doi:10.1175/JPO2885.1.

Klymak, J., R. Pinkel, and L. Rainville (2008), Direct breaking of the internal tide near topography: Kaena Ridge, *J. Phys. Oceanogr.*, *38*, 380–399.

Koch-Larrouy, A., G. Madec, P. Bouruet-Aubertot, T. Gerkema, L. Bessieres, and R. Molcard (2007), On the transformation of Pacific Water into Indonesian Throughflow Water by internal tidal mixing, *Geophys. Res. Lett.*, *34*, L04604, doi:10.1029/2006GL028405.

Kunze, E., and T. B. Sanford (1996), Abyssal mixing: Where it is not, *J. Phys. Oceanogr.*, *26*, 2286–2296, doi:10.1175/1520-0485(1996)026<2286:AMWIIN>2.0.CO;2.

Kunze, E., E. Firing, J. M. Hummon, T. K. Chereskin, and A. M. Thurnherr (2006), Global abyssal mixing inferred from lowered ADCP shear and CTD strain profiles, *J. Phys. Oceanogr.*, *36*, 1553–1576, doi:10.1175/JPO2926.1.

Large, W. G., J. C. McWilliams, and S. C. Doney (1994), Oceanic vertical mixing: A review and a model with a nonlocal boundary-layer parameterization, *Rev. Geophys.*, *32*, 363–403, doi:10.1029/94RG01872.

LeBlond, P. H., and L. A. Mysak (1978), *Waves in the Ocean*, Elsevier, Amsterdam.

Ledwell, J. R., A. J. Watson, and C. S. Law (1993), Evidence for slow mixing across the pycnocline from an open-ocean tracer-release experiment, *Nature*, *364*, 701–703, doi:10.1038/364701a0.

Ledwell, J. R., L. C. St. Laurent, J. B. Girton, and J. M. Toole (2011), Diapycnal mixing in the Antarctic Circumpolar Current, *J. Phys. Oceanogr.*, *41*, 241–246, doi:10.1175/2010JPO4557.1.

Lee, C., E. Kunze, T. B. Sanford, J. D. Nash, M. A. Merrifield, and P. E. Holloway (2006), Internal tides and turbulence along the 3000-m isobath of the Hawaiian Ridge, *J. Phys. Oceanogr.*, *36*, 1165–1183, doi:10.1175/JPO2886.1.

Lozovatsky, I., H. Fernando, and S. Shapolav (2008), Deep-ocean mixing on the basin scale: Inference from North Atlantic studies, *Deep Sea Res., Part I*, *55*, 1075–1089, doi:10.1016/j.dsr.2008.05.003.

Lueck, R. G., and T. D. Mudge (1997), Topographically induced mixing around a shallow seamount, *Science*, *276*, 1831–1833, doi:10.1126/science.276.5320.1831.

Lueck, R. G., F. Wolk, and H. Yamazaki (2002), Oceanic velocity microstructure measurements in the 20th century, *J. Oceanogr.*, *58*, 153–174, doi:10.1023/A:1015837020019.

Lumpkin, R., and K. Speer (2003), Large-scale vertical and horizontal circulation in the North Atlantic Ocean, *J. Phys. Oceanogr.*, *33*, 1902–1920, doi:10.1175/1520-0485(2003)033<1902:LVAHCI>2.0.CO;2.

Lumpkin, R., and K. Speer (2007), Global ocean meridional overturning, *J. Phys. Oceanogr.*, *37*, 2550–2562, doi:10.1175/JPO3130.1.

MacKinnon, J. A., and K. B. Winters (2005), Subtropical catastrophe: Significant loss of low-mode tidal energy at 28.9°, *Geophys. Res. Lett.*, *32*, L15605, doi:10.1029/2005GL023376.

MacKinnon, J. A., T. M. S. Johnston, and R. Pinkel (2008), Strong transport and mixing of deep water through the Southwest Indian Ridge, *Nat. Geosci.*, *1*, 755–758, doi:10.1038/ngeo340.

Marotzke, J. (1997), Boundary mixing and the dynamics of three-dimensional circulations, *J. Phys. Oceanogr.*, *27*, 1713–1728, doi:10.1175/1520-0485(1997)027<1713:BMATDO>2.0.CO;2.

Mauritzen, C., and K. Polzin (2003), Mixing in the Vema Fracture Zone, *Geophys. Res. Abstr.*, *5*, 08601.

Müller, M., H. Haak, J. H. Jungclaus, J. Suendermann, and M. Thomas (2010), The effect of ocean tides on a climate model simulation, *Ocean Modell.*, *35*, 304–313, doi:10.1016/j.ocemod.2010.09.001.

Munk, W. (1966), Abyssal recipes, *Deep Sea Res.*, *13*, 707–730.

Munk, W., and C. Wunsch (1998), Abyssal recipes II: Energetics of tidal and wind mixing, *Deep Sea Res., Part I*, *45*, 1977–2010, doi:10.1016/S0967-0637(98)00070-3.

Nash, J. D., E. Kunze, J. M. Toole, and R. W. Schmitt (2004), Internal tide reflection and turbulent mixing on the continental slope, *J. Phys. Oceanogr.*, *34*, 1117–1134, doi:10.1175/1520-0485(2004)034<1117:ITRATM>2.0.CO;2.

Nikurashin, M., and R. Ferrari (2011), Global energy conversion rate from geostrophic flows into internal lee waves in the deep ocean, *Geophys. Res. Lett.*, *38*, L08610, doi:10.1029/2011GL046576.

Olbers, D. J., M. Wenzel, and J. Willebrand (1985), The inference of North Atlantic circulation patterns from climatological hydrographic data, *Rev. Geophys.*, *23*, 313–356, doi:10.1029/RG023i004p00313.

Osborn, T. R. (1980), Estimates of the local rate of vertical diffusion from dissipation measurements, *J. Phys. Oceanogr.*, *10*, 83–89, doi:10.1175/1520-0485(1980)010<0083:EOTLRO>2.0.CO;2.

Polzin, K. (1999), A rough recipe for the energy balance of quasi-internal waves, in *Aha Huliko'a Hawaiian Winter Workshop*, edited by P. Muller and D. Henderson, pp. 117–128, Sch. of Ocean and Earth Sci. and Technol., Univ. of Hawai'i at Mānoa, Honolulu.

Polzin, K. (2004), Idealized solutions for the energy balance of the finescale internal wave field, *J. Phys. Oceanogr.*, *34*, 231–246, doi:10.1175/1520-0485(2004)034<0231:ISFTEB>2.0.CO;2.

Polzin, K. (2009), An abyssal recipe, *Ocean Modell.*, *30*, 298–309, doi:10.1016/j.ocemod.2009.07.006.

Polzin, K., and E. Firing (1997), Estimates of diapycnal mixing using LADCP and CTD data from I8S, *Int. WOCE Newsl.*, *29*, 39–42.

Polzin, K. L., J. M. Toole, and R. W. Schmitt (1995), Finescale parameterizations of turbulent dissipation, *J. Phys. Oceanogr.*, *25*, 306–328, doi:10.1175/1520-0485(1995)025<0306:FPOTD>2.0.CO;2.

Polzin, K. L., K. G. Speer, J. M. Toole, and R. W. Schmitt (1996), Intense mixing of Antarctic Bottom Water in the equatorial Atlantic Ocean, *Nature*, *380*, 54–57, doi:10.1038/380054a0.

Polzin, K. L., J. M. Toole, J. R. Ledwell, and R. W. Schmitt (1997), Spatial variability of turbulent mixing in the abyssal ocean, *Science*, *276*, 93–96, doi:10.1126/science.276.5309.93.

Richards, K., and S.-P. Xie (2009), Vertical mixing in the ocean and its impact on the coupled ocean-atmosphere system in the eastern tropical Pacific, *J. Clim.*, *22*, 3703–3719, doi:10.1175/2009JCLI2702.1.

Rintoul, S. R., and C. Wunsch (1991), Mass, heat, oxygen and nutrient fluxes and budgets in the North Atlantic Ocean, *Deep Sea Res., Part A*, *38*, S355–S377.

Robinson, A., and H. Stommel (1959), The oceanic thermocline and the associated thermohaline circulation, *Tellus*, *11*, 295–308.

Roemmich, D., S. Hautala, and D. Rudnick (1996), Northward abyssal transport through the Samoan passage and adjacent regions, *J. Geophys. Res.*, *101*, 14,039–14,055, doi:10.1029/96JC00797.

Rudnick, D. L., et al. (2003), From tides to mixing along the Hawaiian ridge, *Science*, *301*, 355–357, doi:10.1126/science.1085837.

Saenko, O. A. (2006), The effect of localized mixing on the ocean circulation and time-dependent climate change, *J. Phys. Oceanogr.*, *36*, 140–160, doi:10.1175/JPO2839.1.

Saenko, O. A., and W. J. Merryfield (2005), On the effect of topographically enhanced mixing on the global ocean circulation, *J. Phys. Oceanogr.*, *35*, 826–834, doi:10.1175/JPO2722.1.

Saenko, O., X. Zhai, W. Merryfield, and W. Lee (2012), The combined effect of tidally and eddy driven diapycnal mixing on the large-scale ocean circulation, *J. Phys. Oceanogr.*, *42*, 526–538.

Simmons, H. L., S. R. Jayne, L. C. St. Laurent, and A. J. Weaver (2004), Tidally driven mixing in a numerical model of the ocean general circulation, *Ocean Modell.*, *6*, 245–263, doi:10.1016/S1463-5003(03)00011-8.

Smith, W. H. F., and D. T. Sandwell (1997), Global sea floor topography from satellite altimetry and ship depth soundings, *Science*, *277*, 1956–1962, doi:10.1126/science.277.5334.1956.

St. Laurent, L. C. (1999), Diapycnal advection by double diffusion and turbulence in the ocean, PhD dissertation, MIT-WHOI Joint Program in Oceanogr., Woods Hole, Mass.

St. Laurent, L. C., and J. Nash (2003), On the fraction of internal tide energy dissipated near topography, in *'Aha Huliko'a Hawaiian Winter Workshop*, edited by P. Muller and D. Henderson, pp. 45–58, Sch. of Ocean ad Earth Sci. and Technol., Univ. of Hawai'i at Mānoa, Honolulu.

St. Laurent, L., and H. Simmons (2006), Estimates of power consumed by mixing in the ocean interior, *J. Clim.*, *19*, 4877–4890, doi:10.1175/JCLI3887.1.

St. Laurent, L. C., and A. M. Thurnherr (2007), Intense mixing of lower thermocline water on the crest of the Mid-Atlantic Ridge, *Nature*, *448*, 680–683, doi:10.1038/nature06043.

St. Laurent, L. C., J. M. Toole, and R. W. Schmitt (2001), Buoyancy forcing by turbulence above rough topography in the abyssal Brazil Basin, *J. Phys. Oceanogr.*, *31*, 3476–3495, doi:10.1175/1520-0485(2001)031<3476:BFBTAR>2.0.CO;2.

St. Laurent, L. C., H. L. Simmons, and S. R. Jayne (2002), Estimating tidally driven mixing in the deep ocean, *Geophys. Res. Lett.*, *29*(23), 2106, doi:10.1029/2002GL015633.

Stow, D. A. (2006), *Oceans: An Illustrated Reference*, Univ. of Chicago Press, Chicago, Ill.

Thurnherr, A. M., L. C. St. Laurent, K. G. Speer, J. M. Toole, and J. R. Ledwell (2005), Mixing associated with sills in a canyon on the midocean ridge flank, *J. Phys. Oceanogr.*, *35*, 1370–1381, doi:10.1175/JPO2773.1.

Toole, J. M. (1998), Turbulent mixing in the ocean, in *Ocean Modeling and Parameterization*, edited by E. Chassignet and J. Verron, pp. 171–190, Kluwer, Dordrecht, Netherlands, doi:10.1007/978-94-011-5096-5_7.

Toole, J. M. (2007), Temporal characteristics of abyssal finescale motions above rough bathymetry, *J. Phys. Oceanogr.*, *37*, 409–427, doi:10.1175/JPO2988.1.

Toole, J. M., R. W. Schmitt, K. L. Polzin, and E. Kunze (1997), Near-boundary mixing above the flanks of a midlatitude seamount, *J. Geophys. Res.*, *102*, 947–959, doi:10.1029/96JC03160.

von Storch, J., H. Sasaki, and J. Marotzke (2007), Wind-generated power input to the deep ocean: An estimate using a 1/10 general circulation model, *J. Phys. Oceanogr.*, *37*, 657–672, doi:10.1175/JPO3001.1.

Waterman, S., A. C. N. Garabato, and K. Polzin (2012), Internal waves and turbulence in the Antarctic Circumpolar Current, *J. Phys. Oceanogr.*, doi:10.1175/JPO-D-11-0194.1, in press.

Weisberg, R., A. Horigan, and J. Knauss (1979), Equatorially trapped Rossby-gravity wave propagation in the Gulf of Guinea, *J. Mar. Res.*, *37*, 67–86.

Winters, K. B., and E. A. D'Asaro (1997), Direct simulation of internal wave energy transfer, *J. Phys. Oceanogr.*, *27*, 1937–1945, doi:10.1175/1520-0485(1997)027<1937:DSOIWE>2.0.CO;2.

Wunsch, C. (1978), The North Atlantic general circulation west of 50 determined by inverse methods, *Rev. Geophys.*, *16*, 583–620, doi:10.1029/RG016i004p00583.

Wunsch, C. (1996), *The Ocean Circulation Inverse Problem*, Cambridge Univ. Press, Cambridge, U. K., doi:10.1017/CBO9780511629570.

Wunsch, C., and R. Ferrari (2004), Vertical mixing, energy and the general circulation of the oceans, *Annu. Rev. Fluid Mech.*, *36*, 281–314, doi:10.1146/annurev.fluid.36.050802.122121.

Wunsch, C., and S. Webb (1979), The climatology of deep ocean internal waves, *J. Phys. Oceanogr.*, *9*, 235–243, doi:10.1175/1520-0485(1979)009<0235:TCODOI>2.0.CO;2.

Wyrtki, K. (1961), The thermohaline circulation in relation to the general circulation in the oceans, *Deep Sea Res.*, *8*, 39–64.

Zhai, X. M., R. J. Greatbatch, and J. Zhao (2005), Enhanced vertical propagation of storm-induced near-inertial energy in an eddying ocean channel model, *Geophys. Res. Lett.*, *32*, L18602, doi:10.1029/2005GL023643.

Zhai, X., H. Johnson, and P. Marshall (2010), Significant sink of ocean-eddy energy near western boundaries, *Nat. Geosci.*, *3*, 608–612, doi:10.1038/ngeo943.